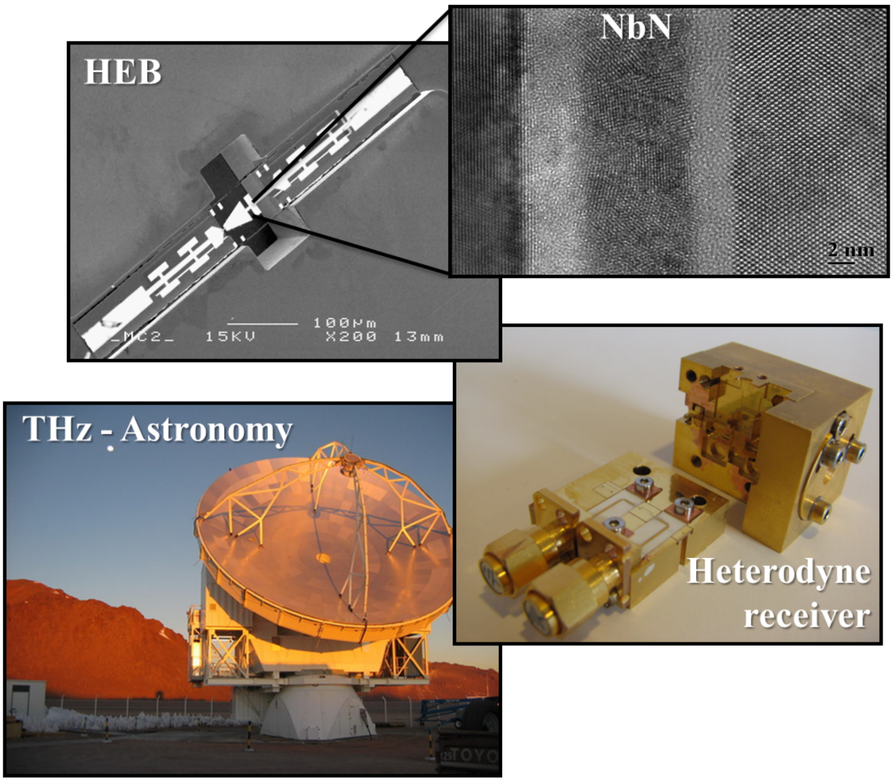


# NbN ultra-thin films for future HEB-based THz systems

*Master Thesis in Wireless, Photonics and Space Engineering*

SASCHA KRAUSE

Department of Earth and Space Sciences
*GARD Group for Advanced Receiver Development*
CHALMERS UNIVERSITY OF TECHNOLOGY
Gothenburg, Sweden 2013

MASTER THESIS IN WIRELESS, PHOTONICS AND SPACE ENGINEERING

# NbN ultra-thin films for future HEB-based THz systems

Master Thesis in Wireless, Photonics and Space Engineering

SASCHA KRAUSE

Department of Earth and Space Sciences

*GARD Group for Advanced Receiver Development*

CHALMERS UNIVERSITY OF TECHNOLOGY

Gothenburg, Sweden 2013

NbN ultra-thin films for future HEB-based THz systems

SASCHA KRAUSE



Master Thesis 2013
Department of Earth and Space Sciences
Division of GARD Group for Advanced Receiver Development
Chalmers University of Technology
SE-41296 Gothenburg
Sweden
Telephone: +46(0)31-772-1846

Cover:
APEX telescope, source: www.panoramio.com/photo/1918447, HEB and receiver [1], HRTEM image taken by Dr. E. Pippel, Max-Planck-Institute Micro-structure physics, Halle, Germany

Chalmers Reproservice
Gothenburg, Sweden 2013

# Acknowledgement

First of all, I would like to thank the head of GARD Victor Belitsky who gave me the opportunity of being part in this fruitful cooperating research group in the promising field of future THz electronics. His support and invitation to the International Symposium on Space Terahertz Technology in Groningen, Netherlands in April 2013 offered me the chance of exchanging knowledge with researchers who contributed with great extend to the present achievement in THz technologies for more than 15years.
I also would like to distinctly thank my supervisor Vincent Desmaris who accompanied me throughout the entire thesis and trained me a lot in mastering the nano-fabrication processes in the mc2 nano-lab which were required for film characterization, analysis and lithography. Furthermore, he provided a pleasant and creative atmosphere and thanks to his collaboration with Dr. Mariusz Rudzinski at the Institute of Electronic Materials Technology Epitaxy Department, Warsaw, Poland who provided numerous high-quality AlGaN epi-layers which were investigated for the prospective deposition of NbN ultra-thin films.
My very experienced co-supervisors Alexey Pavolotsky and Denis Meledin supported me tremendously with important discussions both in theoretical topics and practical issues which were related to mainly super-conductivity, thin-film technolgies and the physics taking place in THz receivers. I honestly appreciate spending a lot of their time for helping me with various measurements and having an open ear whenever I needed it.
The HRTEM images taken at the Max-Planck-Institute für Mikrostrukturphysik in Halle, Germany by Dr. Eckhard Pippel gave me for the first time insight in structures at an atomic level and have been very helpful in the understanding of how to improve NbN ultra-thin films. Furthermore, critical current and field measurements have not been possible without the help of Alexei Kalaboukhov.
I am also grateful about the science-related daily conversations with Phd students at GARD and support of my fellow students by giving me motivation when technical issues occurred.

# Abstract

The key technology for low-noise sub-millimeter and THz receivers lies inevitably in the employment of super-conductive material as the widely used niobium nitride with critical temperature Tc of 16-17K of bulk. However, this material exhibits as well short electron relaxation time which favors its applicability in Hot Electron Bolometers as most sensitive device for heterodyne detection being used above 1.3THz [2].
The enhancement of phonon-cooled HEB's limited IF bandwidth has been a relevant topic since its proposal in 1990 and is associated with the quality of 3.5-6nm thin NbN films. This thesis revisits the concept of employing buffer-layers which have not been utilized yet to deposit NbN onto.
First of all, a reliable deposition process by means of DC magnetron sputtering was set up and yielded to poly-crystalline ultra-thin films on SOI substrate reaching Tc of 10.5K. It has experimentally been verified that, for silicon substrates optimized deposition parameters are transferable to arbitrary substrates which eased the investigation of promising epi-layers such as $Al_xGa_{1-x}N$. As a result, 5.5nm thin NbN films have been successfully deposited onto hexagonal GaN and exhibit Tc as high as 13.2K and RRR close to unity, which is evidence of a high quality single-crystal structure. Furthermore, h-AlGaN layers with different Al content have been studied and clearly show degradation of Tc when the Al content exceeds about 20%. This behavior was confirmed for 3 different deposition temperatures ranging from 650°C to ambient.
The characterization of micro-bridges processed by means of micro-fabrication revealed high uniformity and hardly recognizable deterioration of film's Tc by 0.2-0.3K after processing and storage under ambient atmosphere for one month. Moreover, the critical current density of NbN ultra-thin film grown on GaN and silicon substrates was measured and amounts to about 6MA/cm$^2$ and 2MA/cm$^2$, respectively.
According to the studies of Kaplan [3] on acoustic matching between thin-films and substrates, GaN may provide an enhanced phonon-transmission compared to commonly used substrates. The growth of NbN ultra-thin films at ambient temperatures on GaN substrates has also successfully been demonstrated and offers the ability of highly-integrated THz electronics.

# Contents

# List of Figures

# List of Abbreviations and Symbols

| | |
|---|---|
| ALMA | Atacama Large Millimeter Array |
| SOFIA | Stratospheric Observatory For Infrared Astronomy |
| APEX | Atacama Path Finder Experiment |
| NAOJ | National Astronomical Observatory of Japan |
| ESA | European Space Agency |
| NASA | National Aeronautics and Space Administration |
| HIFI | Heterodyne Instrument for the Far-Infrared |
| SIS | Superconductor-Insulator-Superconductor |
| HEB | Hot Electron Bolometer |
| THz | Terahertz |
| GHz | Gigahertz |
| RF | Radio Frequency |
| IF | Intermediate Frequency |
| LO | Local Oscillator |
| LNA | Low Noise Amplifier |
| QCL | Quantum Cascade Laser |
| IV | Current-Voltage |
| BCS | Bardeen, Cooper, and Schrieffer |
| GLAG | Ginzburg-Landau-Abrikosov-Gor'kov |
| HRTEM | High Resolution Transmission Electron Microscope |
| DC | Direct Current |
| AC | Alternating Current |
| NbN | Niobium nitride |
| AlGaN | Aluminum-Gallium-Nitride |
| SOI | Silicon On Insulator |
| $SiO_2$ | Silicon dioxide |
| LHe | Liquid Helium |
| ADS | Agilent Advanced Design System |

# Notations and Constants

| Notation | Description |
|---|---|
| C | Capacity, thermal or electrical |
| d | Thickness |
| f | Frequency |
| G | Thermal conductivity, gain |
| $H_{c2}$ | Second critical magnetic field |
| $j_{c0}$ | Critical current density |
| P | Power |
| R | Resistance |
| RRR | Resistance ratio $R_{T=300K}/R_{T=20K}$ |
| S | Responsivity |
| $T_C$ | Temperature at which superconductor's resistance drops to 50% of its normal-state value |
| $\Delta T$ | Transition width between 90% to 10% resistance decay |
| $v_t$, $v_l$ | Acoustic velocity transverse, longitudinal |
| $v_F$ | Fermi velocity |
| $\upsilon(0)$ | Density of states |
| $q_t$, $q_l$ | Phonon wave-vector transverse, longitudinal |
| $\lambda$ | Wavelength |
| $\tau_e$ | Characteristic electron cooling time |
| $\tau_{e-ph}$, $\tau_{ph-e}$ | Electron to phonon, phonon to electron relaxation time |
| $\tau_{esc}$ | Escape time of phonons |
| $\omega$ | Angular frequency |
| $\rho$ | Density |
| $\rho_F$ | Fermi momentum |
| $\eta$ | Efficiency, transmission coefficient |

| Constant | Term | Quantity |
|---|---|---|
| $c_0$ | Speed of light in vacuum | 299792458 m/s |
| $\epsilon_0$, $\epsilon_r$ | Permittivity, relative | $8.854 \cdot 10^{-12}$ As/Vm |
| $\mu_0$, $\mu_r$ | Permeability, relative | $1.2566 \cdot 10^{-6}$ Vs/Am |
| $\hbar$ | Planck's quantum | $1.0546 \cdot 10^{-34}$ m$^2$kgs$^{-1}$ |
| $k_B$ | Boltzman constant | $1.38065 \cdot 10^{-23}$ m$^2$kgs$^{-2}$K$^{-1}$ |
| $N_a$ | Avogadro constant | $6.022 \cdot 10^{23}$ mol$^{-1}$ |
| $m_e$ | Mass of electron | $9.1094 \cdot 10^{-31}$ kg |
| $\Phi_0$ | Magnetic flux quantum | $2.0678 \cdot 10^{-15}$ Wb |

# 1 Introduction

The part of the electromagnetic spectrum called sub-millimeter and THz radiation, loosely defined as the frequency range 0.1-3THz and 1-10THz respectively, can be seen as the link where microwaves and optical radiation merge. This allows to take advantage of desirable properties of both frequency regimes simultaneously since the wavelength is small enough to achieve high resolution imaging whereas on the other hand photon's energy is still low on an atomic level and thus not capable of triggering ionization processes. The utilization of this frequency range awoke especially huge interest in astronomical spectroscopy as citing C. Kulesa [4] "It is also one of the most diagnostic, harboring spectral signatures of ions, atoms, and molecules that are central to our understanding of the composition and origin of the Solar System, the evolution of matter in our Galaxy, and the star formation history of galaxies over cosmic timescales.". However, the employment of THz radiation with its desirable features has not been widely utilized yet due to the fact that the absorption by water vapor is extremely high as seen from Fig. (1.1b) which still limits applications in safety, medicine, imaging or communication to short distances.

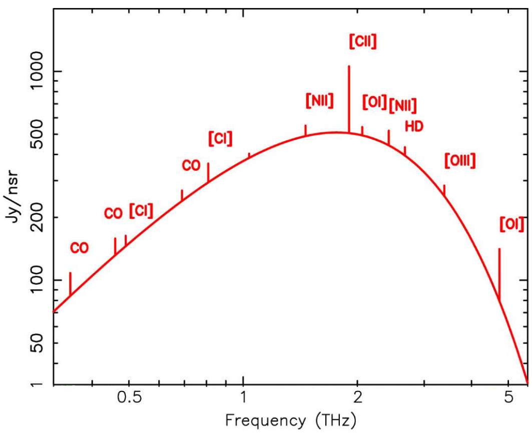


(a) Spectral characteristics of an interstellar cloud at 30K with atomic and molecular spectral lines [4]

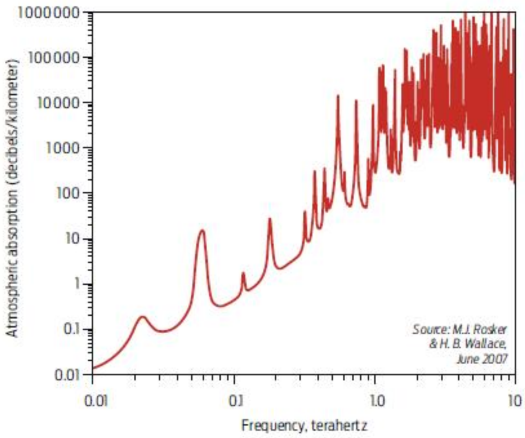


(b) Atmospheric absorption versus frequency [5]

Figure 1.1: THz radiation as revealing tool for astronomical spectroscopy and counteracting atmospheric attenuation

Because of this fundamental limitation astronomical observation platforms in the THz range have been moved to higher altitudes, where the content of atmospheric water vapor is significantly reduced. Recent projects as seen in Fig. (1.2) have come reality due to a wide international network, joint forces and intense ongoing research in this field.

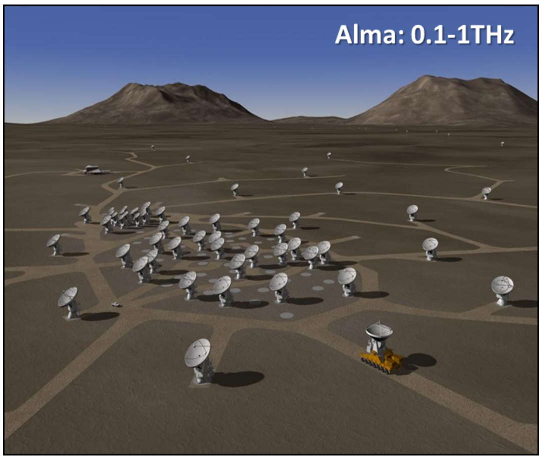


(a) ALMA - Atacama dessert 5058m above sea-level (Source: NAOJ)

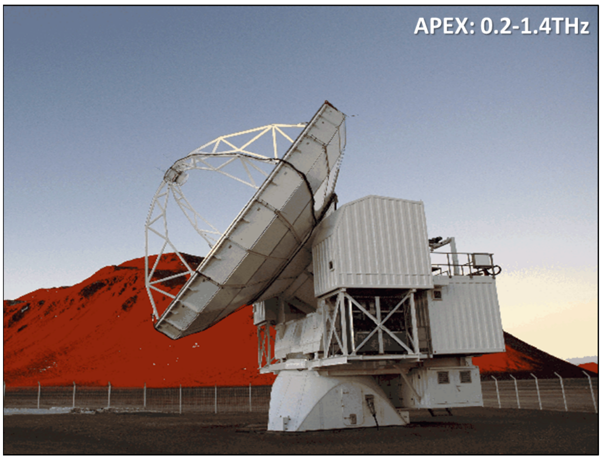


(b) APEX - Atacama dessert 5104m above sea-level (Source: NAOJ)


(c) SOFIA - Airborne observation (Source: NASA)


(d) Herschel - Lower Earth orbit (Source: ESA)

Figure 1.2: Recent projects of sensing THz radiation from elevated locations

Up to now, there exists a wide range of sophisticated detectors capable of sensing THz radiation both operating at room and cryogenic temperatures which have been developed in the last decades. However, only heterodyne receiver systems with high spectral resolution can preserve both phase and amplitude information of the weak incoming radiation by means of mixing it down with a strong LO signal to an easily processable IF band. This enables the spectral analysis of interplanetary objects and reveal informations of the elements they consist of. For astronomical purposes mainly three different receiver technologies are employed for the mixing process such as Schottky diodes and the on a superconducting working principle based SIS tunnel junctions and Hot Electron Bolometer. Despite the fact that SIS tunnel junctions exhibit noise close to the fundamental quantum-limit, the frequency they can operate at is limited and HEB becomes the detector of choice above 1.3THz.

## 1.1 Motivation

Hot Electron Bolometers have no physical limitation in RF frequency bandwidth, are not in need of external magnetic fields and provide easy matching to microwave circuitry due to a purely real impedance. Furthermore, the LO power required for mixing is three to four order of magnitudes lower than Schottky diodes, which overcomes the issue with the lack of frequency-stable solid-state THz local oscillator sources [6]. However, those devices suffer from their limited IF bandwidth which still amounts to maximum reported 8GHz [7] and restrict astronomers in a time-efficient observation.
Many attempts have been made to enhance HEB's IF bandwidth which intrinsically is associated with the quality of the super-conductive ultra-thin NbN films. The single-crystal growth of NbN on MgO is well-established but reliability issues come along with its hydrophilic attitude. Furthermore, sapphire substrates and 3C-SiC epi-layers present as well low lattice-mismatch to NbN and promote an epitaxial growth. However, the afore-mentioned substrates do not provide a sufficient acoustic matching between film and substrates which hinders the phonon escape and eventually limits the IF bandwidth [3], [8]. The substrate of choice from a fabrication point of view is silicon. Well-developed processing techniques allow the integration of additional microwave circuitry such as hybrids and waveguides on the same chip, which is of particular interest for waveguide mixers consisting of thin membrane-like structures. Unfortunately, bare silicon substrates do not favor the epitaxial growth of NbN due to the difference in lattice constant and forfeit superconducting properties of NbN ultra-thin films. The emphasis of this thesis is on the investigation of suitable epi-layers promoting high-quality single-crystal growth of NbN with improved film-substrate interface for enhanced HEB IF bandwidth and further applications in THz electronics.

## 1.2 Structure of the thesis

The next chapter is dedicated to the explanation of the Hot Electron Bolometer working principle and include a thorough investigation of the relaxation process of hot electrons

determining the intrinsic IF bandwidth as well as the role of buffer-layers and their effect on HEB performance enhancement.
The third chapter describes the development of a reliable NbN deposition process by means of reactive DC magnetron sputtering. Several important deposition parameters were identified and yielded to high quality poly-crystalline ultra-thin NbN films on silicon and SOI substrates which will serve as a reference for the ongoing investigation of mainly AlGaN buffer-layers with promising properties as explored in chapter 2.
Many characterization techniques have been applied in order to thoroughly analyze the NbN film properties and relating them to the applicability in HEBs. The conclusion will summarize the main findings of this work and presents next steps towards the employment of the investigated buffer-layers in working HEB devices.

## 1.3 Goal

The goal of this thesis is to investigate the employment of prospective buffer-layers, which have not yet been considered as substrates to deposit ultra-thin NbN films onto. Understanding the process of hot electron relaxation taking place in HEB devices upon THz radiation shall serve as a starting point to deduce advantageous properties which the substrates should exhibit and help to overcome the bottle-neck of limited IF bandwidth of HEB heterodyne receivers. Promising substrates will qualitatively be characterized and compared to state-of-the-art NbN on silicon depositions. Furthermore, the achievement of epitaxially grown ultra-thin NbN films on buffer-layers could also serve other THz electronics based on a superconducting working principle.

# 2 Theoretical Background

## 2.1 Heterodyne detection of THz radiation

The frequency limitation of SIS tunnel junctions arises from their working principle and depends on energy gap $\Delta$ of the super-conducting material being used. When properly biased (e$|V_{bias}|<2\Delta$) Cooper-pairs are broken upon photon-arrival to quasi-particles and tunnel effectively through the few atomic layer thin insulator, widely known as photon-assisted tunneling. Thus, this rapid increase of current exhibit a non-linear IV behavior and is employed as the mixing element of incoming radiation and the LO signal. Principally, SIS devices are based on Nb/Al-AlO$_x$/Nb junctions with $\Delta$=1.45meV which corresponds to a maximal frequency the junction can operate at of about 1400GHz according to $\hbar\omega<4\Delta$. The superconducting tuning circuitry indeed works only lossless until photon energies of 2$\Delta$, which corresponds to 700GHz and losses increase dramatically above this frequency, hence the rise of receiver's noise temperature. The energy gap is linear to the critical temperature with $\Delta(0)=1.764\ k_B$Tc and materials as NbTiN or NbN with $\Delta\approx$2.5meV have been considered in order to extend the maximum operating frequency up to about 1.4THz.
Schottky diodes are based on a semiconductor-metal junction and the mixing occurs due to its non-linear current-voltage characteristics as well. Although, they are too noisy for astronomical applications Fig. (2.1a), require significant more LO power to operate them and therefore suffer from the lack of pure solid-state LO sources as presented in Fig. (2.1b).
As depicted in Fig. (2.2) and (2.3) , the fundamental difference between the commonly employed microwave receiver architecture and THz low-noise system is the presence of a LNA at the front-end of the receiver chain.

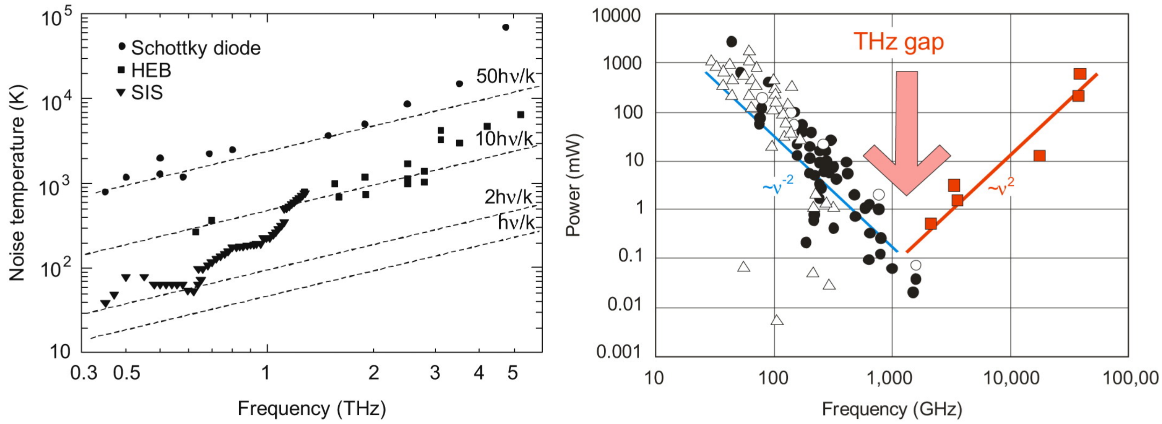


(a) Heterodyne low-noise receivers (b) LO solid-state sources (□ QCL, ○ frequency multipliers, △ other)

Figure 2.1: Receiver noise-temperature and availability of LO sources [6]

It mainly determines the overall noise performance of the entire receiver since the noise contribution of all following components are divided by the LNA gain.

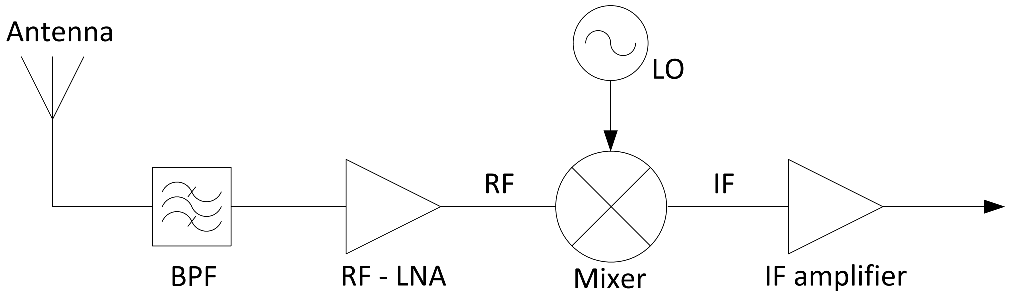


$$T_{system} = T_{Ant} + T_{BPF} + T_{RF-LNA} + \frac{T_{Mix}}{G_{RF-LNA}} + \frac{T_{IF-LNA}}{G_{RF-LNA}G_{Mix}}$$

Figure 2.2: Ordinary microwave system architecture

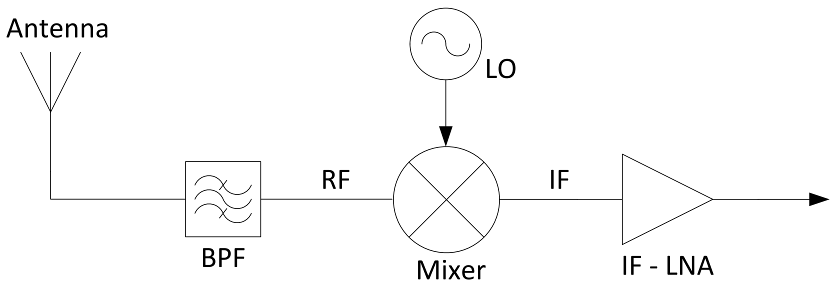


$$T_{system} = T_{Ant} + T_{BPF} + T_{Mix} + \frac{T_{LNA}}{G_{Mix}}$$

Figure 2.3: Sub-millimeter and THz receiver architecture

When going beyond about 100GHz, LNAs do not usually provide sufficient gain and low-noise performance and the system overall noise-temperature becomes smaller when placing the mixer component at the front-end of the receiver chain as seen in Fig. (2.3). This matter of fact motivates the keenness of low-noise mixer development, especially for astronomical observations.

## 2.2 Thermal Detectors - Bolometers

A bolometer can be considered as a thermometer which senses the temperature change of an absorber upon incoming radiation. Presupposing a temperature-dependent behavior of its resistance, the alteration can electrically be detected as a voltage swing. As seen from Fig. (2.4a) two heat reservoirs are present, the surrounding heat-sink held at a certain bath-temperature $T_{bath}$ and the temperature T of the thermally conductive attached bolometer with heat capacity C. .

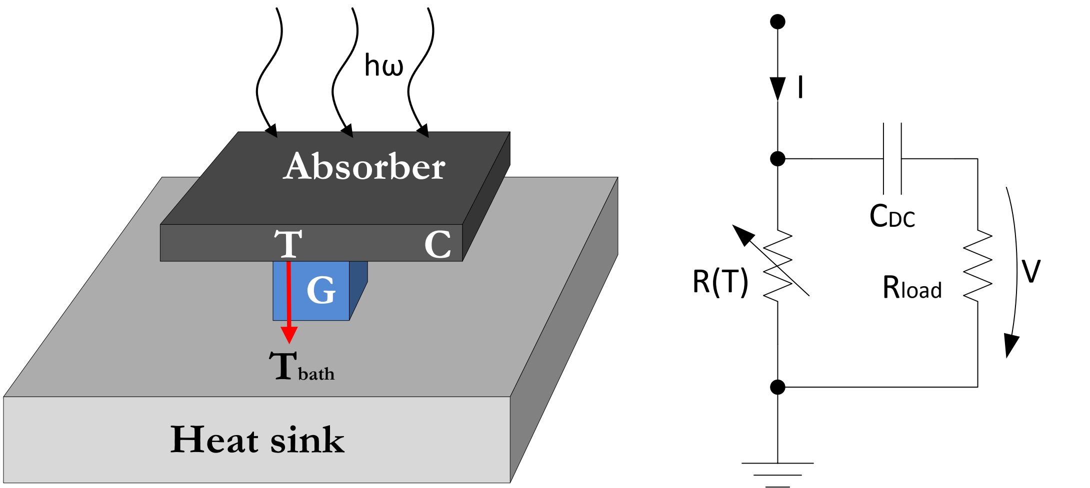


(a) Schematic of a bolometer (b) Electrical read-out circuitry

Figure 2.4: Working principle of bolometers

The general working principle can be derived from the thermal balance Eq. (2.1) and their solutions upon the case of steady power flow as well as under stopped radiation.

$$P = C\frac{dT}{dt} + G\left(T - T_{bath}\right) \tag{2.1}$$

$$T = \begin{cases} T_{bath} + \frac{P}{G} & \text{steady radiation } P = const. \\ T_{bath} + \frac{P}{G} \cdot e^{-\frac{t}{\tau}} & \text{stopped radiation } P \to 0 \end{cases} \tag{2.2}$$

$$\text{with} \quad \tau = \frac{C}{G} \tag{2.3}$$

The bolometer response time $\tau$ characterizes the speed of the device and is calculated from the ratio of bolometer's heat capacity C and thermal conductivity G of the thermal link to the surrounding heat-sink Eq. (2.3). The electrical read-out is performed as simplified illustrated in Fig. (2.4b). A constant current is driven through the temperature-dependent resistance of the bolometer and evoke a certain DC power dissipation. Under chopped incoming radiation with modulation frequency $\omega$ the dissipated power alters and a voltage swing can be coupled through the DC-block capacitor and appears across a resistive load. Thus, the responsivity of the bolometer is also defined as the change in voltage drop per watt of absorbed power $S_A$=dV/dP [V/W].

In order to improve the responsivity, superconducting materials have been employed in Transition Edge Sensors TES since the transition from the superconducting state to the normal-state resistance exhibit extraordinary high dR/dT ratios and yield to very low-noise performance due to the operation at cryogenic temperatures as depicted in Fig. (2.5).

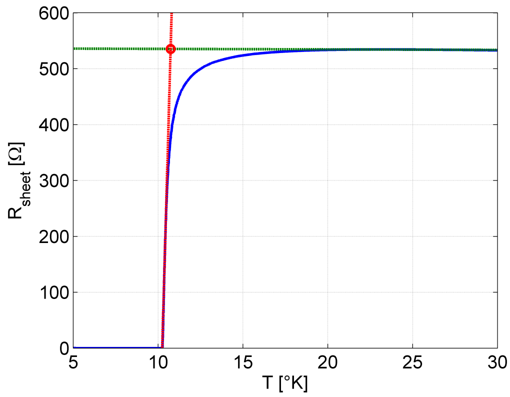


(a) Transition from normal-state to superconducting state

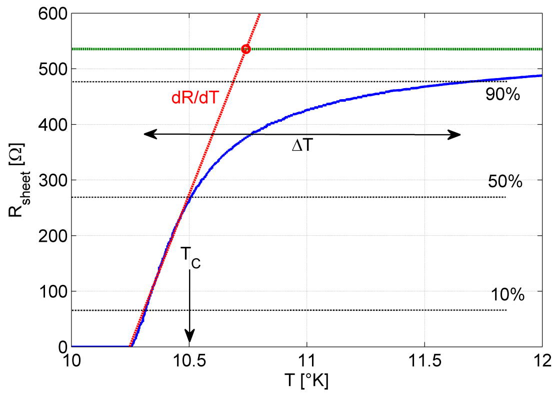


(b) Zoomed transition

Figure 2.5: Resistance versus temperature behavior of ultra-thin NbN film on silicon substrate

TES bolometers operate close to zero Kelvin and provide an efficient detection of photons in a wide frequency range. Although, they are quite slow devices with characteristic time constants in the milli- to microsecond regime, i.e. the SCUBA-2 TES array with about 1ms [9].
Reducing the time constants of bolometers to nanoseconds and less by utilizing the hot electron effect, which is present in some materials, made the bolometer capable of operate as a frequency mixer device as firstly demonstrated by Gershenzon et al. in 1990 [11]. The principle of NbN Hot Electron Bolometer found widely approval and was refined in the last decades. The fundamental working principle of HEB will be thoroughly discussed in the following section.

## 2.3 Hot Electron Bolometer mixer

### 2.3.1 Working principle

In a conventional bolometer the incoming radiation is absorbed by the entire absorber medium and involves the heating of both lattice and electrons. In the case of HEB indeed only quasi-particles or electrons in a thin superconducting film are thermalized even before an energy exchange with its lattice is possible. Subsequently, the relaxation of heated electrons takes place by either out-diffusion to the contact-pads or by exchanging energy to the film lattice and furthermore to the substrate, held at the bath temperature. The first mentioned, also known as diffusion-cooling is present in materials with high diffusion constants and require bolometer bridge dimensions in the order of electrons mean free path in order to effectively transfer energy from electrons to the as heat sink serving contact pads. A HEB mixer based on this working principle has firstly been demonstrated in 1993 [12]. However, the reliable fabrication of bolometer bridge dimensions in the order of 100nm as required for Nb HEB is challenging and the phonon-cooled HEB principle established for practical astronomical applications.

Thus, only the phonon-cooling mechanism will be explained by taking the example of NbN.

As seen from Fig. (2.6a) the thin superconducting film is driven into the transition region between super-conducting and normal-state by means of LO power when in a mixer mode as well as DC power dissipation. In the vicinity of Tc only a small amount of Cooper-pairs is present and un-paired electrons behave as normal quasi-particles.
Fig. (2.6b) illustrates the situation upon incoming radiation.The quasi-particles are thermalized within a short time amounting to about $\tau_{e-e}$<6.5ps for NbN [13], [14]. The

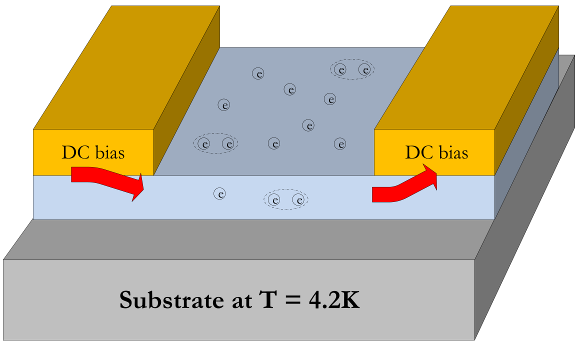


(a) DC and LO bias provide operating point on the transition to the resistive state

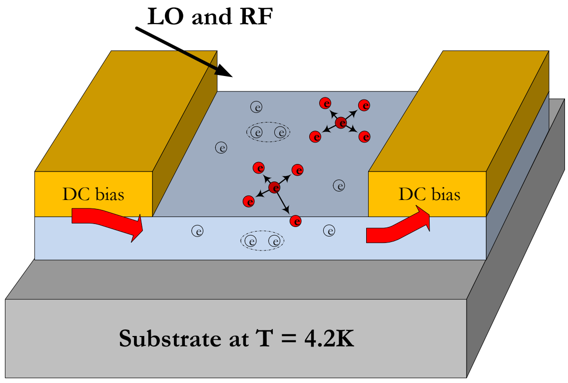


(b) Fast thermalization of electrons upon absorbed radiation within $\tau_{e-e}$

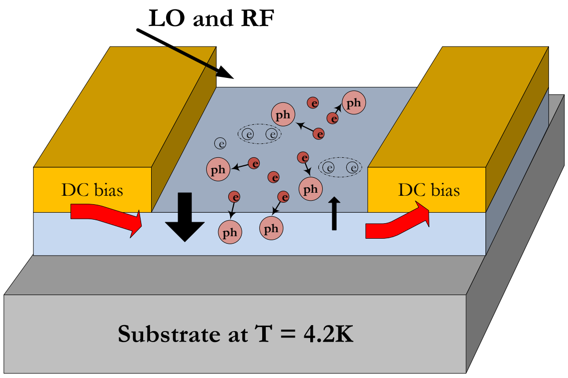


(c) Energy exchange of hot electrons to phonons within $\tau_{e-ph}$

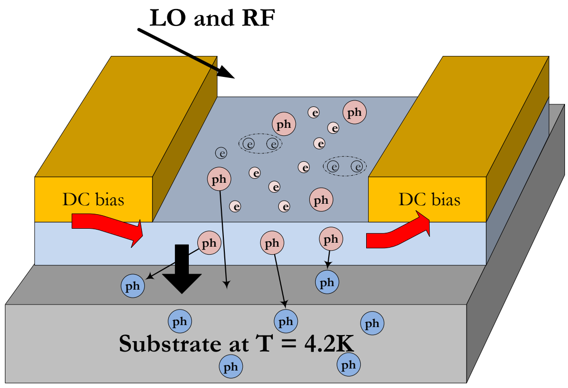


(d) Most phonons escape into the substrate within $\tau_{esc}$, small amount of energy exchange back to electrons within $\tau_{ph-e}$

Figure 2.6: Phonon cooling mechanism in HEB mixer

following figure depicts the relaxation process of heated electrons to the film lattice which takes place within the characteristic electron-phonon time $\tau_{e-ph}$. However, a small portion of excited phonons will re-exchange energy to electrons as quantified by Eq. (2.4).

$$\tau_{e-ph} = \tau_{ph-e} \frac{C_e}{C_{ph}} \tag{2.4}$$

The ratio of electron and phonon capacity amounts to about $C_{ph}/C_e$=6.5 for NbN [13]. Furthermore, the substrate held at bath temperature serves as heat sink for the phonons, which relax through the interface across film and substrate within the escape time $\tau_{esc}$. It is worth mentioning that in the case of $\tau_{esc}>\tau_{ph-e}$ a bolometric response can be observed since electron and phonon subsystem exhibit equal temperatures.

Briefly summarized the non-equilibrium Hot Electron effect is present under following conditions.

- Rapid thermalization of electrons
  $\tau_{e-e} \ll \tau_{e-ph},\ \tau_{ph-e},\ \tau_{esc}$
- Preventing the back-flow of energy from phonons to electrons by short escape times into the substrate
  $\tau_{esc} \ll \tau_{ph-e}$

The importance of the non-equilibrium state and fast "average" cooling rate as expressed in Eq. (2.5) taken from [15], [16] eventually allows the HEB operating as a heterodyne mixing element.

$$\tau_e = \tau_{e-ph} + \left(1 + \frac{C_e}{C_{ph}}\right)\tau_{esc} \tag{2.5}$$

### 2.3.2 Frequency mixing in HEBs

The superposition of the electrical fields of both applied LO-signal at $\omega_{LO}$ and weak incoming radiation $\omega_{RF}$, respectively, determines the total power absorbed in the HEB. The electrical fields with amplitudes $A_{RF}$ and $A_{LO}$ are defined according Eq. (2.6), (2.7).

$$E_{RF}(t) = A_{RF} \cdot cos(\omega_{RF}t) \tag{2.6}$$

$$E_{LO}(t) = A_{LO} \cdot cos(\omega_{LO}t) \tag{2.7}$$

and the resulting absorbed power P(t) under a certain coupling efficiency $\alpha$ between the radiation and the film

$$\begin{aligned} P(t) &\propto \alpha\,(E_{RF} + E_{LO})^2 + P_{DC} \\ &\propto \alpha\Bigg(A_{LO}^2 \cdot cos^2(\omega_{LO}t) + A_{RF}^2 \cdot cos^2(\omega_{RF}t) + \\ &\qquad + 2\left[A_{LO}A_{RF} \cdot cos(\omega_{LO}t) \cdot cos(\omega_{RF}t)\right]\Bigg) + P_{DC} \end{aligned} \tag{2.8}$$

with $2cos^2(x) - 1 = cos(2x)$ and $cos(x \pm y) = cos(x)cos(y) \mp sin(x)sin(y)$

$$\begin{aligned} P(t) \propto P_{DC} &+ \frac{A_{LO}^2}{2} + \frac{A_{LO}^2}{2} \cdot cos(2\omega_{LO}t) + \frac{A_{RF}^2}{2} + \frac{A_{RF}^2}{2} \cdot cos(2\omega_{RF}t) + \\ &+ A_{LO}A_{RF} \cdot cos\left((\omega_{LO} + \omega_{RF})t\right) + A_{LO}A_{RF} \cdot cos\left((\omega_{LO} - \omega_{RF})t\right) \end{aligned} \tag{2.9}$$

As seen from Eq. (2.5) the highest frequency $\omega$=1/$\tau_e$ which the HEB can respond to lies in the order of GHz. A thorough study of relaxation times in NbN HEB was conducted in 1999 by means of short laser-pulse radiation and extracted $\tau_{e-ph}$=10ps, $\tau_{ph-e}$=65ps and $\tau_{esc}$=38ps yielding to about 5.3GHz IF bandwidth for a device with critical temperature of 10.5K [14]. Thus, it is clearly visible that a HEB device is simply too slow to follow the frequency components 2$\omega_{RF}$, 2$\omega_{LO}$ and ($\omega_{RF}$+$\omega_{LO}$) from Eq. (2.9) which amount to be above 2THz if the HEB operates at 1THz and only the IF frequency component $\omega_{IF}$ = |$\omega_{LO}$-$\omega_{RF}$| is modulating the temperature of the HEB as summarized in Eq. (2.10).

$$P(t) = P_{DC} + \underbrace{\alpha\left(\frac{A_{LO}^2}{2} + \frac{A_{RF}^2}{2}\right)}_{\overline{P_0}} + \underbrace{A_{LO}A_{RF}\cdot cos\left(|\omega_{LO} - \omega_{RF}|t\right)}_{P_{IF}\cdot cos(\omega_{IF}t)} \tag{2.10}$$

A more realistic evaluation of device's gain IF bandwidth can be conducted when taking into account the self-heating due to dissipated bias power and the positive feedback effect of the resistive load. The self-heating enhances the response time of the HEB and the noise temperature and conversion-efficiency under practical assumptions can be estimated [17].

## 2.3.3 Hot-electron relaxation process

This section is dedicated to clarify the overall relaxation process of hot electrons due to the incoming radiation. The so-called cooling rate of different subsystems being involved such as electron-electron, electron-phonon and phonon-substrate interactions determine eventually the intrinsic IF bandwidth, the HEB can be working at.

### 2.3.3.1 Electron-phonon system

Many theoretical and experimental results have been published about the electron-phonon interaction in disordered metal films for very low temperatures where the metals can be considered as being in the impure case or "dirty". A figure of merit to distinguish between the "dirty" or "clean" limit is the product of phonon wave-vector times the electron-mean-free path $q_t l \ll 1$ or $q_t l \gg 1$, respectively, with $q_t = k_B T/\hbar v_t$. Furthermore, the interactions in the dirty limit is very much dependent on the kind of vibrating scatterers (see detail in [16], [18]). According to [19] the electron-phonon time can be expressed for $q_t l \ll 1$ as following:

$$\tau_{e-ph}^{-1} = \underbrace{\frac{\pi^4 T^4 l}{5\rho_F^2}\left[\frac{\beta_l}{v_l^3} + \left(1 - \frac{l}{L}\right)\frac{3\beta_t}{2v_t^3}\right]}_{\text{longitudinal phonons}} + \underbrace{\frac{3\pi^2 T^2}{2\rho_F^2 L}\left[\frac{\beta_l}{v_l} + \left(1 - \frac{l}{L}\right)\frac{2\beta_t}{v_t}\right]}_{\text{transverse phonons}} \tag{2.11}$$

and kinetic constant of electron-phonon interaction $\beta$ [16], [20]:

$$\beta_l = \left(\frac{2}{3}\epsilon_F\right)^2 \frac{\upsilon(0)}{2\rho v_l} \tag{2.12}$$

$$\frac{\beta_t}{\beta_l} = \left(\frac{v_l}{v_t}\right)^2 \tag{2.13}$$

The term l/L depicts hereby the electron-mean-free path with respect to the non-vibrating potential. As long as vibrating impurities (defects, film/substrate interface) move along the same way as host atoms ($L \to \infty$) the interaction with transverse phonons is negligible and a temperature dependence of $T^4$ has been widely observed at very low temperatures [18]. Indeed, as scatterers are vibrating, the electron-phonon interaction can be significantly enhanced by means of inelastic scattering and yields to a $T^2$ dependence. However, in order to apply this theory for NbN films the condition $q_l l \ll 1$ needs to be satisfied. The lower and upper limit of the temperature regime of interest is defined by the bath temperature of liquid helium 4.2K and the operating point of the HEB amounting to about the critical temperature of NbN thin films 7-13K, respectively. The electron-mean-free path can be assumed to be in the order of 1nm for ultra-thin

NbN films [16], [10] and thus belong to the disordered metal films in the dirty limit. However, the work of Ptitsina [20] describes the electron-phonon interaction also in the range of moderate disorder in the regime between the "dirty" and "clean" limit. This theory is also applicable for high quality NbN ultra-thin films used for HEB since the product $q_t$l amounts to 0.15 - 0.45 and $q_l$l to 0.08 - 0.25 for temperatures 5K - 15K and transverse and longitudinal sound velocities of 7800m/s and 4200m/s, respectively [29].

$$(\tau_{e-ph,l})^{-1} = \frac{7}{2}\pi\zeta(3)\beta_l \frac{(k_B T)^3}{\hbar\,(\rho_F v_l)^2} F_l(q_l l) \tag{2.14}$$

$$(\tau_{e-ph,t})^{-1} = 3\pi^2\beta_t \frac{(k_B T)^2}{(\rho_F v_t)\,(\rho_F l)} F_t(q_t l) \tag{2.15}$$

For temperatures much smaller than the Debye temperature, the limits of $F_l(q_l l)$ are given by Eq. (2.16) and (2.17).

$$F_l(q_l l) = \begin{cases} 1, & l \gg \hbar v_l / k_B T \\ \frac{2\pi^3}{35\zeta(3)}(q_l l), & l \ll \hbar v_l / k_B T \end{cases} \tag{2.16}$$

$$F_t(q_t l) = \begin{cases} 1, & l \gg \hbar v_t / k_B T \\ \frac{\pi^2}{10}(q_t l), & l \ll \hbar v_t / k_B T \end{cases} \tag{2.17}$$

Now, assuming a temperature of T=10K one can compute the product $\hbar v_l/k_B T$ = 6nm and $\hbar v_t/k_B$ T = 3.3nm, respectively. By comparing those lengths with the mean-free-path of electrons of about 1nm, one can see that the films do not behave as being clearly in the "dirty" limit and exact computation of $F_l(q_l l)$ and $F_t(q_t l$ would be required. Principally, the longitudinal sound velocity is greater than the transverse in disordered metal films and from Eq. (2.14) and (2.14) the main contribution to the interaction is attributed to transverse phonons.
Introducing the elastic transport time which is simply expressed by the electron mean-free path divided by the fermi velocity $v_f$ Eq. (2.18) from [20]

$$\tau = \frac{l}{v_f} \tag{2.18}$$

The inelastic electron-phonon interaction is due to transverse interaction which allows to simplify the evaluation to Eq. (2.19).

$$\tau_{e-ph,t}^{-1} = \frac{9}{8} B T^2 F_t(q_t l) \tau^{-1} \tag{2.19}$$

$$\text{with} \qquad B \approx \frac{4\pi^2 \beta_t}{3\epsilon_F \rho_F v_t} k_B^2 \tag{2.20}$$

However, the mean interaction time of the electron-phonon subsystem can be calculated without neglecting the longitudinal contribution by Eq. (2.21).

$$\tau_{e-ph} = \left( \frac{1}{\tau_{e-ph,t}} + \frac{1}{\tau_{e-ph,l}} \right)^{-1} \tag{2.21}$$

An attempt was made to compute the intrinsic electron-phonon relaxation time of NbN films from its physical properties and turned out to be in accordance with the work of [21], [22], [23] which include a thorough investigation of ultra-thin NbN HEB and the electron-phonon cooling processes taking place.

One can already draw some first conclusions from the theoretical considerations in order to tune film properties towards enhanced electron-phonon cooling later on. As stated earlier the main contribution to the scattering and therefore to the hot electron relaxation process is attributed to transverse phonons. As seen from Eq. (2.15) or (2.19) the interaction time follows a linear electron-mean-free path l and a theoretical $T^{-2}$ temperature dependence, respectively. Polycrystalline NbN films usually exhibit a much higher resistivity than epitaxially grown ones which can be accompanied with a reduction of electron-mean-free path and theoretical increase of interaction rate if held at the same temperature [24]. However, this could not be observed since the density of states $\upsilon(0)$ of those films decreases with increasing resistivity which eventually lowers the interaction rate, see Eq. (2.12) and no enhancement can be achieved [25]. An effective influence can only be exerted by increasing the temperature the HEB is working at, in turn increasing the critical temperature of the ultra-thin NbN film. Although a theoretical $\tau_{e-ph} \propto T^{-2}$ dependence is predicted in reality a $\tau_{e-ph} \propto T^{-1.6}$ has been observed [17]. This consideration points towards an epitaxial growth of high quality NbN films which exhibit high Tc and thus favors the electron-phonon interaction process.

#### 2.3.3.2 Phonon-substrate escape

The next important step is to evaluate the characteristic time needed to exchange the elevated phonon temperature in the film to the bath temperature that the underlying substrate is held on. This process is known as the phonon escape into the substrate and is only dependent on the film thickness d, the acoustic matching coefficient $\eta$ as average of the longitudinal and transverse transmission coefficient and the velocity of sound in the film. Later on, it will be shown that the escape time is as important as the electron-phonon interaction since both have the same order of magnitude (near 10K and films thinner 10nm of the order of ten picoseconds [16]) and need to be considered together to draw conclusions about the overall relaxation process of heated electrons and moreover the response of the bolometer itself. Again from [3] and [19] the escape time is simply defined as in Eq. (2.22)

$$\tau_{es} = \frac{4d}{\eta v_m} \tag{2.22}$$

and remains for instance independent of the ambient temperature or specific heat capacities of the quasi-particle or phonon system. The mean velocity of sound can be evaluated by Eq. (2.23).

$$v_m = \frac{1}{3}\left(\frac{1}{v_l^3} + \frac{2}{v_t^3}\right)^{-\frac{1}{3}} \tag{2.23}$$

Measurements of mechanical properties of NbN in order to extract both longitudinal and transverse acoustic velocities are rare. Although they seem to be consistent as seen from Tab. (2.1).

| Elastic Constants | | | Extracted acoustic velocities | | | Reference |
|---|---|---|---|---|---|---|
| $C_{11}$ [GPa] | $C_{12}$[GPa] | $C_{44}$[GPa] | $v_l$ [m/s] | $v_t$[m/s] | $v_m$[m/s] | |
| 696.2 | 112.6 | 85.9 | 7762 | 4241 | 4730 | [26] |
| 498 | 212 | 89 | 7454 | 3803 | 4261 | [27] |
| 604 | 223 | 184 | 8764 | 5158 | 5717 | [27] |
| 556 | 152 | 125 | 7808 | 4511 | 5007 | [28] |
| 705 | 115 | 82 | 7761 | 4193 | 4680 | [29] |

Table 2.1: Compilation of mechanical NbN properties measured by several groups

The average sound velocity for NbN is about 4900 m/s according to the presented references and will be used in later calculations.

The acoustic transmission coefficient and its derivation will be described more thorough in the following section. From [16] and [23] one can see that the escape time amounts to about 160ps for 20nm and 38ps for ≈3.5nm NbN film, respectively and is in accordance with the proportionality of thickness Eq. (2.22). However, enhancing the relaxation process of film phonons to the substrate cannot be achieved by reducing the thickness to less than about 3.5nm since for such thicknesses the super-conductivity in NbN is suppressed and the resistivity rises when approaching the coherence length of the material. The evolution of Tc of epitaxially grown NbN films versus film thickness in the range from 100nm to 2.5nm has recently been reported and mechanisms as the weak localization and Coulomb interaction, the proximate effect as well as the quantum size effect or electron wave leakage model have been taking into account to explain this process, see Fig. (2.7)

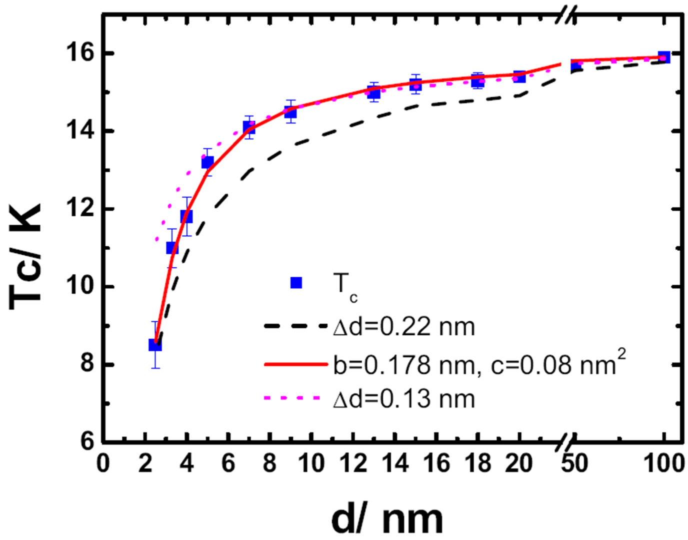


Figure 2.7: Critical temperature versus thickness for epitaxially grown NbN films on MgO substrates from [30]

### 2.3.4 Practical HEB

The impedance of the HEB for very high frequencies can be chosen by the bolometer dimensions according the aspect ratio of length and width times film's sheet resistance $R_{RF}=R_\square \cdot L/W$. This enables the designer to easily match HEB both to quasi-optical antennas or systems based on waveguides. When the device is used as a heterodyne receiver, the LO power requirement is determined by its volume. The bias point on HEB's IV curve exhibiting lowest noise-temperature will be selected and features a characteristic IF impedance close to the differential resistance dV/dI in this specific operation point.

The studies of Nebosis et al. [17] allow under certain simplification the estimation of important HEB parameters such as the noise-temperature, the conversion efficiency as well as the IF gain bandwidth taking into account the self-heating and positive feedback effect of the bias circuitry.

### 2.3.5 Use of buffer layers

It is evidence that high quality as well as ultra-thin films which exhibit at the same time high Tc are favorable to achieve ultimate HEB performance in particular with respect to the IF bandwidth. The quality of growth of NbN films relies more and more on the underlying substrate the film is deposited onto when going to films as thin as 3.5nm. Commonly used substrates providing epitaxial growth of ultra-thin NbN are MgO and sapphire reaching critical temperatures up to 12K and 13.3K, respectively [30], [31]. The requirements a buffer-layer has to satisfy in order to provide improved film-quality are numerous. In general, one wants to aim for lowest lattice-mismatch to reduce stress, tension in the film and interface as well as support the growth of a single-crystal epitaxial phase. This enables high Tc and narrow transition from the normal to super-conductive state which is favorable for enhanced IF bandwidth as well as sensitivity. Buffer-layers on silicon serving this purposes are poly-crystalline MgO [32] or recently demonstrated 3C-SiC [33],[34] and made it possible to attain Tc as high as Tc=12K for 4-5nm thin films. Rarely taken into account is the interface across substrate and NbN film which mainly determines the relaxation from film-phonons to the substrate described as acoustic transmission coefficient. The acoustic properties of silicon, MgO, sapphire or 3C-SiC are fairly similar and do not provide an effective acoustic matching to NbN which eventually yield for certain angles to phonon-trapping in the film and reduces the overall-relaxation process linked to limited IF bandwidth. Thus, an investigation of different substrates was conducted and the acoustic matching qualitative evaluated by applying the acoustic mismatch theory according to Kaplan [3]. The phonon transmission coefficient $\eta$ is derived by Snell's Law while neglecting the effect of phonon attenuation and dispersion as well as assuming the film and substrate to be isotropic solids. This work particularly describes the estimation of the afore-mentioned phonon transmission coefficient of super-conductive thin films and various substrates.

$$\frac{sin\Phi_1}{v_{l1}} = \frac{sin\Phi_2}{v_{l2}} = \frac{sin\gamma_1}{v_{t1}} = \frac{sin\gamma_2}{v_{t2}} \tag{2.24}$$

with $\Phi$ and $\gamma$ with respect to the z-axis. Longitudinal and transverse waves generate at the boundary between two media, in particular super-conductive film and substrate, both pairs of refracted and transmitted longitudinal and transverse waves.

$$\eta = \left(\frac{2\eta_t}{v_t^2} + \frac{\eta_l}{v_l^2}\right)\left(\frac{2}{v_t^3} + \frac{1}{v_l^3}\right)^{-\frac{2}{3}} \tag{2.25}$$

| substrate | lattice | | acoustic velocity | | density | total reflection | | dielectric |
|---|---|---|---|---|---|---|---|---|
| | a [Å] | c [Å] | $v_l/v_{NbN}$ | $v_t/v_{NbN}$ | $\rho$ [g/cm$^3$] | $\theta_{c,l}$ [°] | $\theta_{c,t}$ [°] | $\epsilon_r$ |
| NbN[a] | 4.4 | - | 1 | 1 | 8.47 | - | - | - |
| Si[b] | 5.43 | - | 1.14 | 1.22 | 2.33 | 61 | 55 | 11.7 |
| $SiO_2$[e] | amorphous | | 1.5 | 1.4 | 1.8-2.2 | 42 | 46 | 3.9 |
| AlN[b,f] | 3.11 | 4.98 | 1.42 | 1.39 | 3.26 | 45 | 46 | 8.5 |
| AlGaN[b,f] | ↓ | ↓ | 1.16 | 1.07 | 4.71 | ↑ | ↑ | ↓ |
| GaN[b,f] | 3.19 | 5.19 | 0.98 | 0.88 | 6.15 | - | - | 8.9 |
| Sapphire[c] | 4.79 | 12.99 | 1.26 | 1.34 | 3.91 | 53 | 48 | 11.3/9.5 |
| MgO[d] | 4.22 | - | 1.25 | 1.21 | 3.58 | 53 | 56 | 9.8 |
| 3C-SiC[b] | 4.36 | - | 1.2 | 0.94 | 3.17 | 56 | - | 9.72 |
| 4H-SiC[b] | 3.07 | 10.05 | 1.58 | 1.62 | 3.211 | 39 | 38 | 9.66 |

Table 2.2: Acoustic matching related properties of several substrates

The ratio of the sound velocities in film and substrate as well as their density ratio is determining the acoustic transmission coefficient. Taken data for NbN from Tab. (2.1) and substrates from Tab. (2.2) are indicated in Fig. (2.8) below.

However, as described previously the main contribution of phonon- interaction is attributed to transverse phonons. This case is as well mentioned in [3] and poor matching of transverse phonons can be considerably improved by choosing a substrate/film combination with $v_{t2}/v_{t1}$ smaller than unity as well as $\rho_2/\rho_1$ greater unity whereas the latter condition is not as important as the first one. Furthermore, fulfilling these conditions will avoid the effect of phonon trapping inside the film due to total internal reflection at the interface. The most promising material which can be found from Tab. (2.2) is GaN due to the highest density ratio among suitable substrates and velocity ratio close to unity. Looking at commonly used substrates as silicon, MgO or sapphire which show low density ratios and sound velocities of 1.28, 1.27 and 1.40 higher than the ones in NbN, respectively will lead to phonon-trapping and deteriorate eventually the overall hot electron cooling process. As previously explained epitaxy is favorable over polycrystalline growth and can only be achieved if the lattice-mismatch between NbN and substrate is small. Tab. (2.2) also provides lattice constants for several buffer-layer and epitaxial growth has been demonstrated and is well established for MgO, sappire and 3C-SiC substrates. However, the lattice of AlGaN compositions both in their cubic and hexagonal crystal-structure matches the one of NbN in its [100] and [111]-orientation as well and may be a promising candidate to grow epitaxially onto. In addition the grow

[b] http://www.ioffe.ru/SVA/NSM/Semicond [f] [35] [c] [36] [d] [37] [e] [38] [a] see Tab. (2.1)

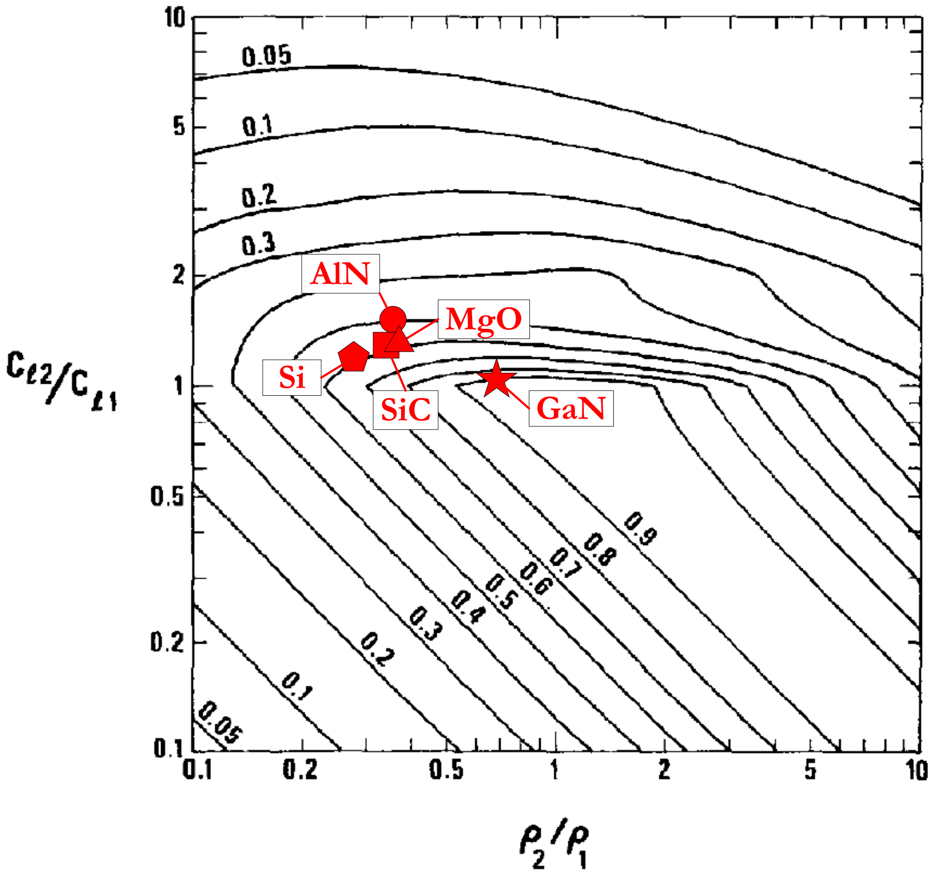


Figure 2.8: Contours of longitudinal phonon transmission coefficient $\eta_l$ [3]

of NbN and NbTiN onto AlN buffer-layer has recently been demonstrated resulting in improved Tc compared to bare silicon substrates [39] indeed no attempt has ever been made to use the believed advantageous properties of GaN and its little lattice-mismatch.

### 2.3.6 Film/Substrate interface

In addition to the idealized phonon transmission coefficient, one has to take into account a non-ideal interface between film and substrate which may deteriorate the interaction process. A study of phonon-transmission across lattice-mismatched interfaces has recently been conducted for Si/Ge-like materials and can qualitatively be applied for epitaxially grown NbN structures [40].

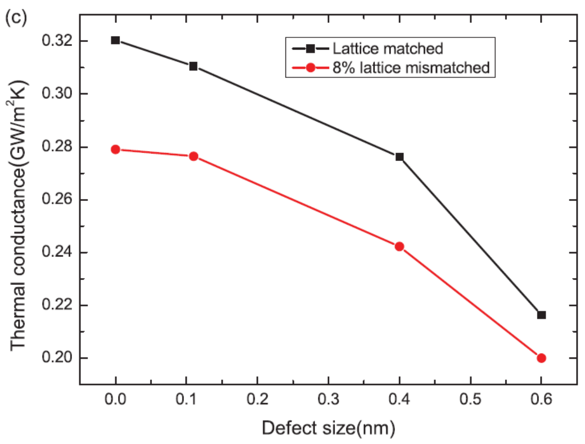


(a) Thermal conductance versus defect size and lattice mismatch

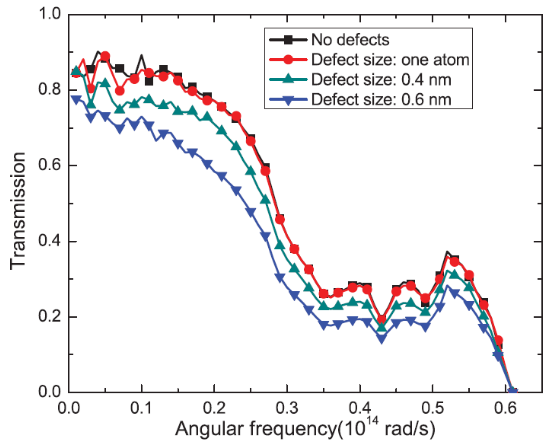


(b) Phonon transmission

Figure 2.9: Phonon transmission dependence on lattice mismatch and defect size at Si/Ge interface from [40]

Depicted in Fig. (2.9a) is the dependence of thermal conductance, which in turn is an equivalent to the relative phonon transmission, as a function of defect size at the interface for both the lattice matched and mismatched case. The effect of defect size across the interface turned out to overcome the influence of the difference in lattice-matching on the transmission properties for increasing defect sizes. This is supported by further experiments with an alloyed layer at the interface and a reduction in thermal conductance with increasing layer thickness. Fig. (2.9b) additionally illustrates the effect of defect size versus phonon- frequency [40].

This study on Si/Ge like interfaces may reveal general dependences on phonon transmission properties affected by defects across the interface and deterioration due to lattice-mismatch which are transferable to the NbN/substrate system. Thus, one can say that lattice-matched substrates and high-quality interfaces without defects such as stress, atomic reconstruction or species mixing is favorable for the effective escape of film phonons into the substrate.

# 3 Ultra-thin film deposition of NbN

The deposition of NbN thin-films is usually conducted by means of reactive DC magnetron sputtering and requires a carefully understanding of the processes taking place.

## 3.1 Optimization of deposition parameters

This chapter casts light on numerous deposition parameters such as illustrated in Fig. (3.1), which turned out to influence the superconducting properties of ultra-thin NbN films.

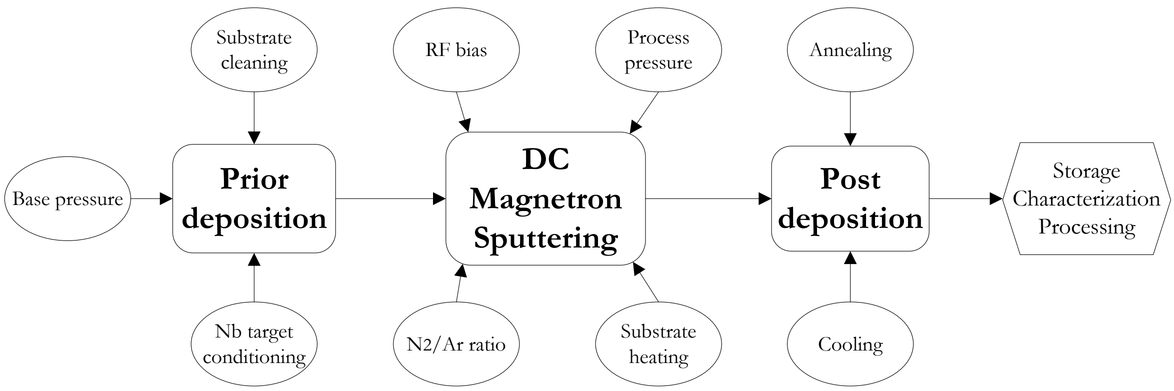


Figure 3.1: Critical temperatures for NbN grown on silicon as a function of $N_2$/Ar for different pressure and substrate temperatures

The experiment was partly organized as a fractional design (DOE) in order to exclude possible interaction effects for example of substrate heating, $N_2$/Ar ratio and process pressure.

### 3.1.1 General deposition procedure

The deposition of our films was performed in the AJA 3160 DC magnetron sputtering tool. Prior loading, an ultra-sonic cleaning procedure in Isopropyl Alcohol (IPA) was

conducted in order to remove organics and small particle residues from the film surface. Furthermore, a two-step Argon plasma cleaning sequence was applied prior transferring the samples from the load-lock system into the process-chamber. The latter procedure maintained the high-vacuum quality of about $2\cdot10^{-8}$Torr in the process-chamber achieved by the turbo-pump. Both depositions at ambient and elevated temperatures were performed, whereas rotation of the substrate holder yielded to high uniformity of substrate temperature and deposition rate across the entire area.
Moreover, after transferring the substrate holder, an additional plasma cleaning step prior-deposition was applied and the Nb target with 99.95% purity pre-sputtered for about 3-4min at closed shutter. During this time the substrate holder was already held at a certain temperature unless an ambient temperature deposition was conducted. This provided an uniform heat contribution and enabled the substrate itself to adopt to the chosen temperature.

## 3.1.2 DC magnetron sputtering of NbN

The actual sputtering process of Nb in a reactive $N_2$/Ar atmosphere held at a certain pressure and deposition rate mainly determines the stoichiometry of the grown NbN composition. It is worth mentioning that many different phases of $Nb_xN_y$ have been observed but only the tetragonal $Nb_4N_{3x}$ $\gamma$-phase and the face-centered (fcc) $NbN_{1-x}$ $\delta$-phase exhibit superconductivity at 12-15K and 15-17.3K for bulk, respectively [41], [42]. The latter one is of exceptional interest for phonon-cooled HEB as explained earlier and the aim will be to synthesize it in a pure manner.

### 3.1.2.1 Reactive atmosphere

The partial pressure of nitrogen cannot be chosen independently of deposition rate as well as process pressure and needs to be adjusted over time due to target degradation in order to attain a proper film stoichiometry. It is not fully resolved whether the reactive reaction of Nb and N takes place at the Nb target or at the surface of the substrate itself. The Fig. (3.2) below illustrates the evolution of Tc of NbN thin film son silicon substrates under certain process pressure and substrate holder temperatures as a function of N2/Ar.

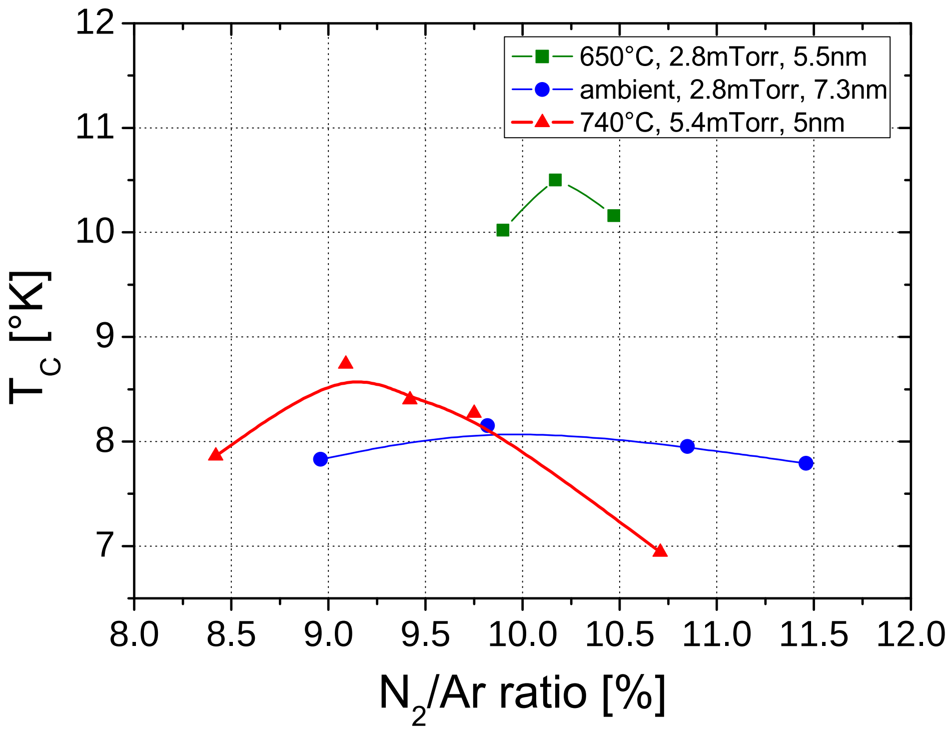


Figure 3.2: Critical temperatures for NbN grown on silicon as a function of $N_2$/Ar for different pressure and substrate temperatures

High quality films with Tc as high as 10.5K on SOI (green curve) exhibit a narrow range with optimal stoichiometry and degrade quickly apart from this. The depositions carried out without intentional substrate heating (blue curve) shows a smooth curve shape and indicates a poly-phase composition due to less available activation energy for ordering and crystallization at the substrate surface. Furthermore, one may point out that the optimum $N_2$/Ar composition turned out to be slightly higher at lower deposition pressures than at higher. This shift was as well observed and reported in [43]. Taking advantage of slightly increased deposition rates and longer mean-free path of sputtered Nb atoms implying higher energies at the surface for low pressure deposition yielded eventually to improved microscopic and macroscopic film properties as increased Tc, narrower transition from the normal to the super-conductive state as well as lower resistivity which is an evidence of more order and less residues enclosed in film's crystal structure. Fig. (3.3) illustrates the polycrystalline appearance of thin NbN films deposited at ambient temperatures for pressures of 2.8mTorr and 5.4mTorr, respectively.

---

[a] Dr. Eckhard Pippel at Max-Planck-Institute für Mikrostrukturphysik, Halle, Germany

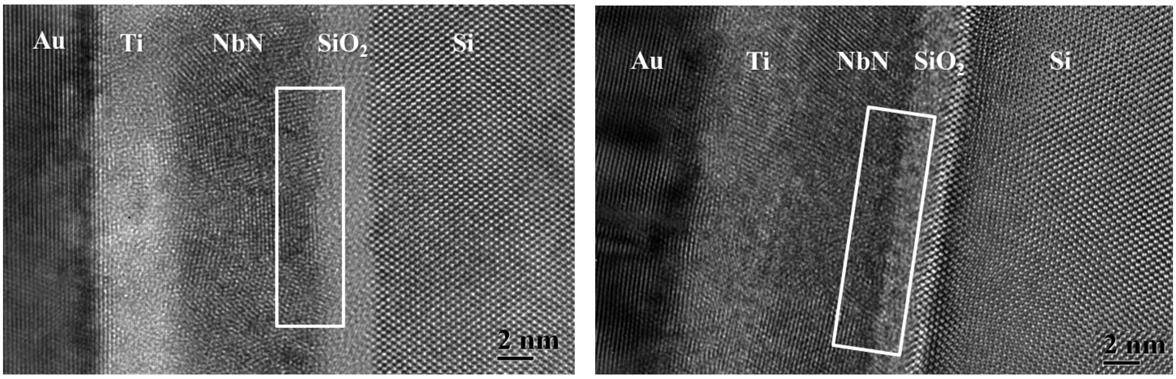


(a) Process-pressure: 2.8mTorr

(b) Process-pressure: 5.4mTorr

Figure 3.3: HRTEM[a] of polycrystalline NbN films grown at ambient temperatures onto silicon-substrates

The interface across $SiO_2$ and the NbN film (white-rimmed) appears much more uniform and with less defects at 2.8mTorr as the ones deposited at 5.4mTorr. Furthermore, the measured resistance of the films from Fig. (3.3) turns out to be increased by about 50% for the film deposited at higher pressure after correction for the difference in thickness of 7.3nm and 6.1nm, respectively. Drawing the conclusion that those films made under lowered pressure will as well exhibit better acoustic matching and phonon transmission due to the improved interface across film and substrate.

#### 3.1.2.2 Substrate heating

Substrate heating is applied to enhance the mobility of Nb atoms at the substrate surface and as a consequence thereof achieving more ordered films and improved chrystalinity. Several experiments were conducted to figure out whether there is an optimal temperature range achieving both high Tc, low normal-state resistance and narrow transition width. Fig. (3.4) illustrates the critical temperature as well as the RRR figure-of-merit for a polycrystalline NbN film deposited onto SOI substrate.

A gradual increase of substrate temperature gives rise to improved Tc as well as RRR since the available energy and mobility at the surface is increased. This trend continues to about 650°C where it reaches a maximal Tc of about 10.5K and decreases then for higher temperatures. This behavior can be attributed to a significant rise of enclosures in the film and is evidentially seen in highly deteriorated RRR ratio. A reasonable explanation for this could be the out-gassing of the substrate holder and worsening of the base pressure. It has also been observed that the pressure in the process-chamber post deposition was noticeable higher than for lower substrate temperatures and almost as low as prior deposition for unheated substrates.

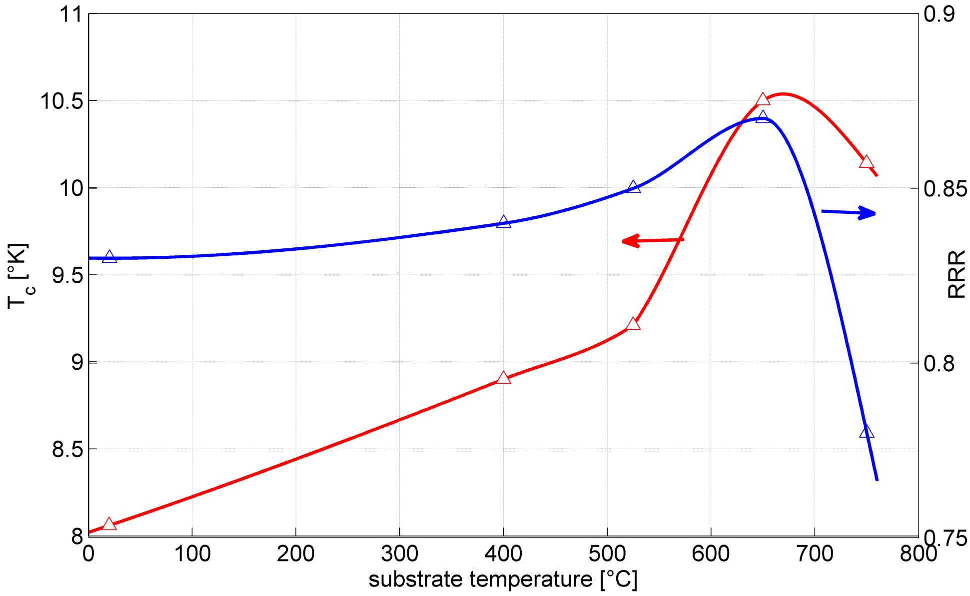


Figure 3.4: Critical temperatures and RRR of ≈5.5nm NbN on SOI as a function of substrate temperature

#### 3.1.2.3 RF bias

The motivation of introducing RF power to the plasma while sputtering can be explained by supporting positive charged Ar-ions with additional energy close the surface of the film. The frequency is fixed to about 13MHz and low enough for Ar-ions to follow the electrical field. The energy applied to the ions is effectively transferred to the film surface by means of ion bombardment and supports the ordering of NbN. This technique is particularly useful when only little surface energy is available as in the case for unheated substrate holders. Different experiments were conducted and reveal that the presence of additional RF bias is already essential and changes in Tc for varying power of 3W to 6W could not be observed. Although, films with thickness of 5.5nm deposited at elevated temperatures exhibited Tc as low as 6K when no RF bias was applied in comparison with those at 4W RF and Tc at about 9K under the same deposition conditions, which highlights the essentiality of this deposition parameter.

### 3.1.3 Post deposition treatment

After the deposition process the films are cooled down from elevated substrate temperatures and ready for their characterization. Several attempts have been made to post-anneal NbN-films by means of thermal treatment as Rapid Thermal Annealing RTA [44], [45]. Although, it turned out that additional heat treatment of NbN films deteriorates its properties which has been confirmed in this work. Furthermore, it was previously concluded that the deposition at elevated substrate temperatures increases Nb mobility and supports the more ordered growth on the other hand the enclosure of impurities in the film rose drastically above 750°C. This fact prompt to investigate film's properties when held at high temperatures in vacuum, argon and nitrogen atmospheres under various pressure, similar conditions as found post-deposition.

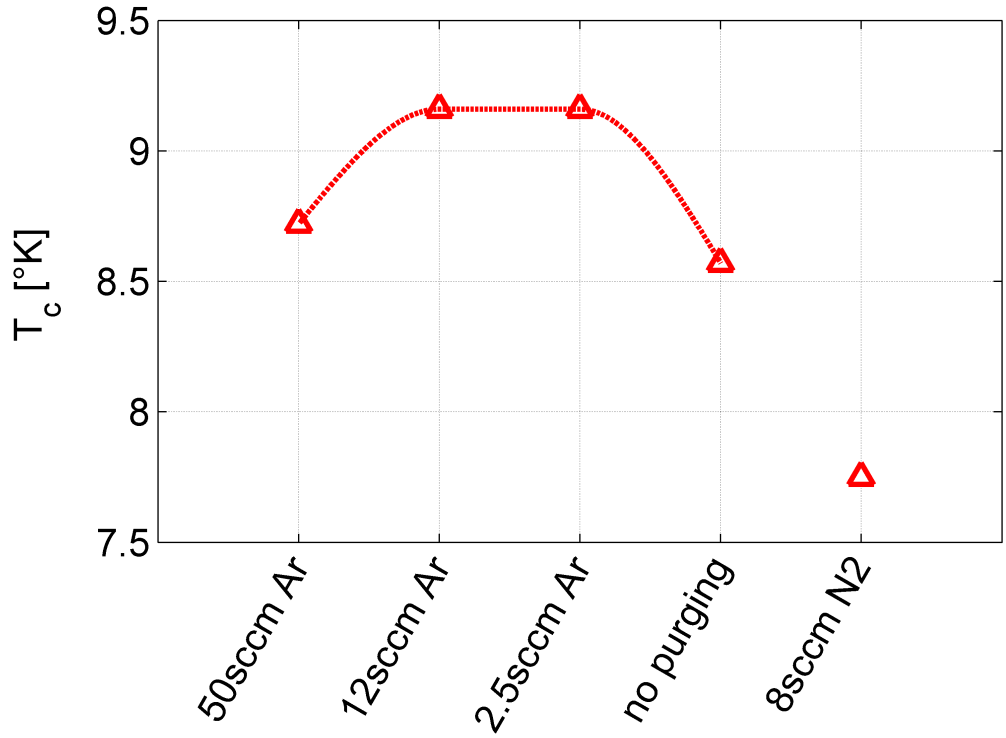


Figure 3.5: Effect of different atmospheres and flows while cooling down the hot deposited films

As illustrated in Fig. (3.5) films exposed to an argon atmosphere post-deposition shows a clearly higher Tc than those cooled in vacuum or nitrogen. The introduction of argon at low pressure seems to purge effectively impurities from the vicinity of the still hot remaining film which otherwise would lead to contamination. However, the purging with nitrogen gas at elevated temperatures may affect the stoichiometry of NbN and yield to the deteriorated Tc depicted in Fig. (3.5)

## 3.2 Thickness characterization using ellipsometry

Ellipsometry is a well-developed, sensitive and non-destructive optical tool for the analysis of thin-films. Polarized light is reflected on the surface of single or multiple stacked layers and the change in phase over a certain wave-length range measured. The complex refractive index can reveal important physical properties and even in the case of NbN a studies was published identifying a $\Psi$-dependence on film's bulk critical temperature ranging from 6-16K [46]. However, the purpose of ellipsometry in this work serve the confirmation of thicknesses and the assumed presence of a $Nb_2O_5$ natural oxide layer on top. Several measurements on $NbN/SiO_2/Si$ were conducted since the optical properties of silicon substrates are well-characterized which eased the extraction of the thickness of NbN.

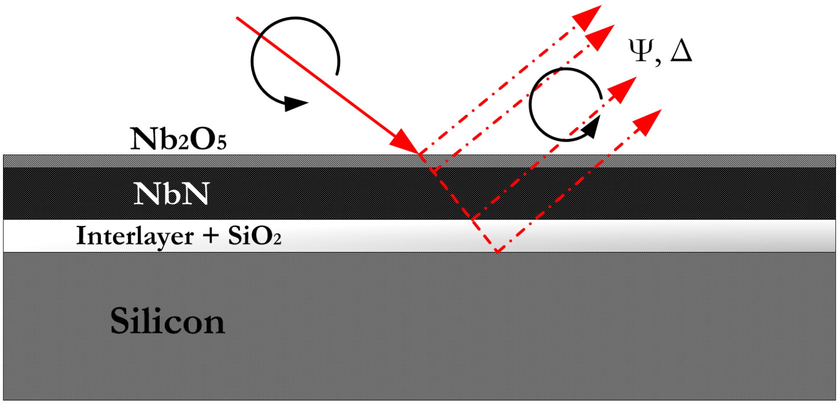


Figure 3.6: Applied structure in order to fit layer thicknesses in measured ellipsometry data

A reliable model of NbN was issued using a harmonic oscillator approach and fine-tune their coefficients. The model from Fig. (3.6) fitted well to the measured data depicted in Fig. (3.7) and provides a good consistency of thickness taken over several samples as summarized in Tab. (3.1)

| Dep. time [s] | Tc [K] | Thickness [nm] $SiO_2$+Interlayer | Thickness NbN [nm] scaled to HRTEM | Thickness NbN [nm] fitted to ellipsometry |
|---|---|---|---|---|
| 45 | 10.5 | 4 | 5.3 | 5.48 |
| 45 | 10.2 | 4 | 5.3 | 5.64 |
| 45 | 10 | 4 | 5.3 | 5.55 |
| 38 | 9.75 | 4 | 4.5 | 4.4 |
| 45 | 10.05 | 3.33 | 5.3 | 6 |

Table 3.1: Fitted thicknesses from ellipsometry scans

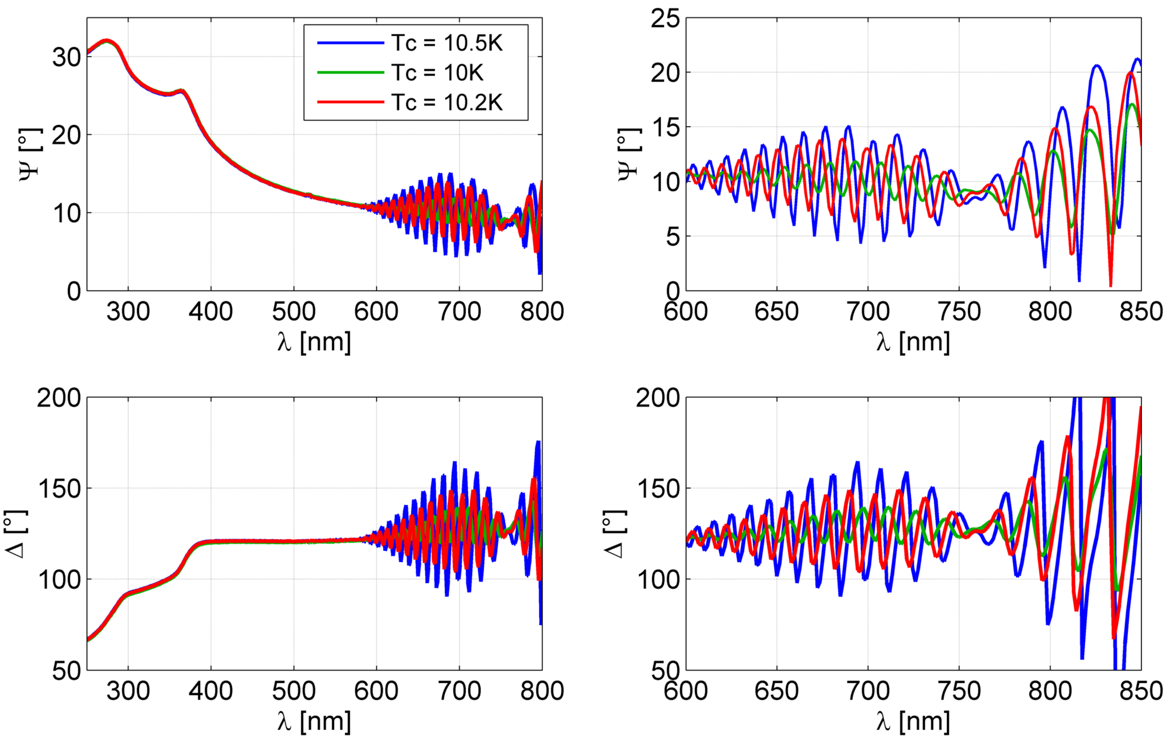


Figure 3.7: Plotted phase components from 250nm to 850nm with 70° angle of incidence

The oscillating phase behavior as seen in the zoomed extract in Fig. (3.7) for wavelengths greater the 600nm is most-likely attributed to the SOI substrate. The top-layer of silicon is in the order of $\mu$m and corresponds under a certain angle to a multiple of the wavelength where the oscillation begins. Silicon changes its optical properties from opaque in the visible spectrum to transparent for longer wavelength, which pronounces the effect. Furthermore, the oscillations in the phase do not appear for NbN films on bulk silicon substrates which supports the statement. However, it turned out that the deviation of the amplitude of oscillation goes along with different resistivities of the NbN films being investigated and shown in Fig. (3.7). The amplitude gets highest for films with higher Tc and least resistivity whereas NbN exhibiting lower Tc and higher resistivity clearly show reduced oscillations. This is interpreted as higher quality films with less impurities exhibit less damping of the light that shines through and occur visible in the ellipsometry data. This observation is reinforced when comparing the spectra of films being cooled down in argon or vacuum as discussed previously. The latter one shows much smaller magnitude of the oscillating envelope corresponding to a higher film resistance, respectively.

# 4 Results and discussion

This chapter is dedicated to the characterization of NbN ultra-thin film deposited onto substrates as AlN, hexagonal $Al_xGa_{1-x}N$ and GaN buffer-layer grown on sapphire and silicon-substrates as well as bulk GaN in order to exclude stress effects arising from the buffer-layer itself. All depositions on afore-mentioned substrates are compared with high-quality films on silicon or SOI-substrates, which also serve as an indicator for possible changes of deposition parameters over time.

## 4.1 Transferability of deposition conditions from Si to arbitrary substrates

First of all, it needed to be proven that the deposition conditions of NbN do not change for different substrates in order to confirm a proper comparability between them when deposited at the same time. Thus, the following substrates were used and the partial pressure of $N_2$ similarly to Fig. (4.2) changed. The critical temperature of the films was characterized by a R(T) four-probe-measurement system with an calibrated temperature sensor.

Illustrated in Fig. (4.2a) slight changes of the $N_2$/Ar gas composition effectively influences film's stoichiometry and deteriorate the critical temperature especially for elevated substrate holder temperatures as observed earlier. Moreover, it turns out that all films reach their maximum Tc at a certain ratio amounting to about 10.2%. The conclusion can be drawn that the investigated substrates are equally affected by stoichiometric changes and therefore allowing a direct comparison of films deposited at the same time. It is also worth mentioning that both poly-crystalline and AlN/AlGaN substrates with wurtzite-crystal structure seem to be up to the highest investigated temperature since a potential release of nitrogen or diffusion of aluminum at the interface would have been indicated as shifted $N_2$/Ar response and deteriorated Tc as compared to silicon.

The important parameter substrate heating was investigated and a series of deposition at temperatures from 400-750°C performed. All samples were lying in close vicinity on

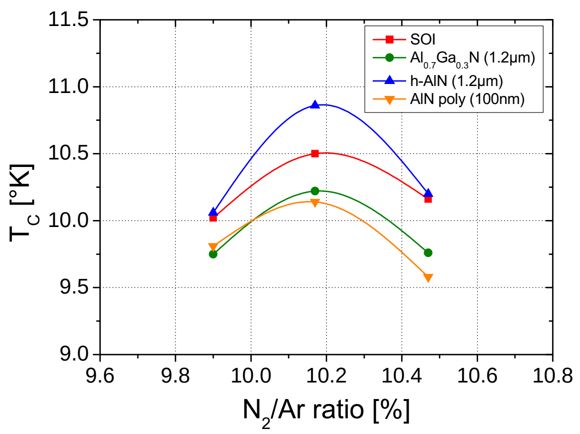


(a) Tc as function of changed $N_2$/Ar ratio

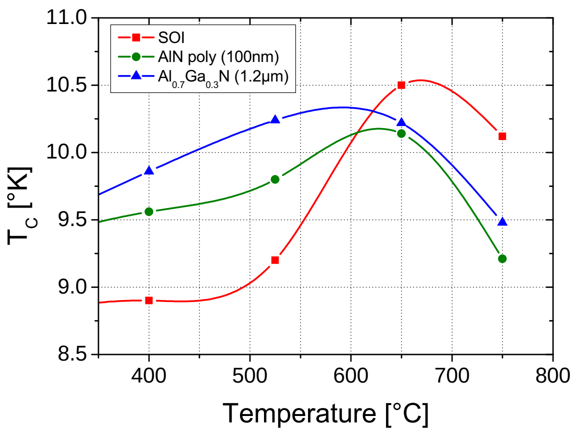


(b) Substrate heating and evolution of Tc

Figure 4.1: Film stoichiometry and substrate temperature dependence for different substrates

the substrate holder and held for 5 minutes prior deposition at the chosen temperatures in order to assure them to be equally heated.

Depicted in Fig. (4.2b) the effect of intentional substrate heating differs between films deposited onto SOI, AlN and AlGaN, respectively. The most suitable deposition temperature for high Tc films can be achieved at about 550-650°C. However, the films on AlN and h-AlGaN do not exhibit such a strong dependence on optimized substrate temperature during the deposition process than the one grown onto silicon-substrates.

## 4.2 Hexagonal AlGaN buffer-layer

High quality $Al_xGa_{1-x}N$ layer on sapphire substrates with thickness of about $1.2\mu$m and gradually increase in Al content were grown at ITME in Poland. The growth of 5.5nm NbN ultra-thin films was performed under conditions that found out to be optimal for the deposition on silicon-substrates and as previously shown are transferable to arbitrary substrates.

The deposition was performed at ambient, 525°C and 650°C which turned out to be the most relevant temperature ranges to observe changes in film's quality. Fig. (4.2a,b) give Tc and RRR as a function of different Al content in the film which in turn can be seen as gradual modulation of the lattice constant. The measured film area was about 12x6mm characterized by means of four-point-probe-measurement. Film's quality can easily be assessed by looking both at Tc and RRR. These figures-of-merit correlate whereas a RRR close to unity give evidence of a epitaxial growth which is desirable for most applications. Furthermore, when holding the substrate temperature at about 525°C the degradation

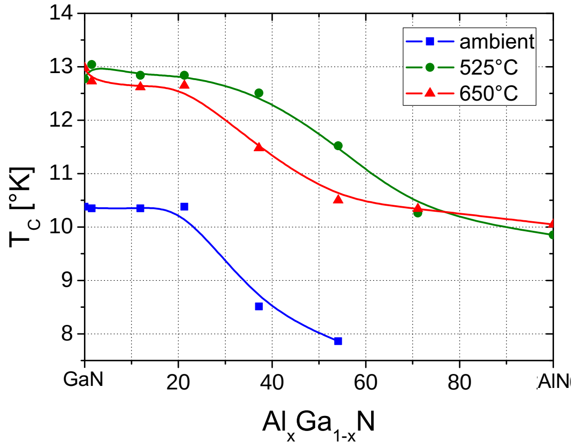


(a) Tc

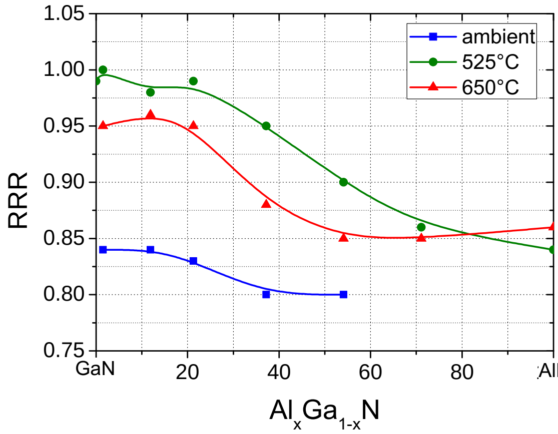


(b) RRR

Figure 4.2: Tc and RRR as assessing quality factors for AlGaN-substrates compared to high-quality depositions on silicon

of film quality with Al content takes place over a wider range of Al variation than the ones deposited at 650°C which may be attributed to increased enclosure of residues. This statement is supported by an increased sheet resistance observed for those films. On the other hand films deposited without intentional substrate heating exhibit Tc as high as 10.4K for substrates with Al content ranging from 0-20%. Although, the lack of energy at the surface does not enable the growth of a single epitaxial phase.
Furthermore, it is not fully understood whether RF bias rather suppress the formation of epitaxy or supports it. Therefore, the following experiment was conducted. A NbN film assumed to be about 4.5nm from linearly scaling of deposition time from a HRTEM investigated sample with certain thickness, was conducted and compared to one under same deposition conditions but without applied RF bias of about 4W.

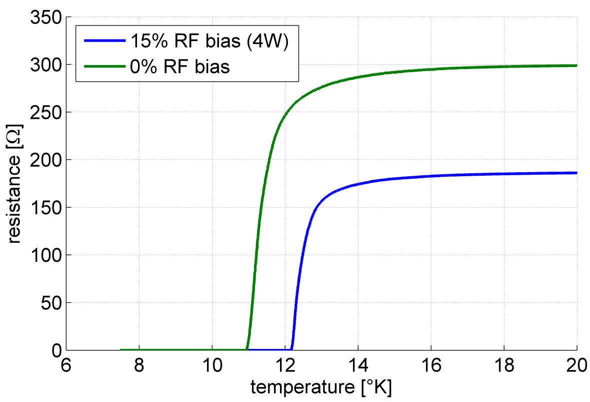


Figure 4.3: Influence of RF bias on epitaxially grown NbN (≈4.5nm) on GaN buffer-layer

From Fig. (4.3) it is clearly seen that RF bias during the sputtering process promotes the growth of a high-quality NbN epitaxial composition resulting in improved Tc and lowered resistance. It needs to be mentioned that the deposition rate may slightly change under different RF bias power this indeed does not explain the large deviation and can certainly be neglected. It is assumed that plasma generated by the additional RF power provides a cleaner environment and less impurities can be built in NbN's crystal structure. A similar behavior has been observed for silicon-substrates.

### 4.2.1 Comparison of NbN ultra-thin films on various buffer-layers

The outstanding results in terms of Tc and RRR as figure-of-merits on h-GaN buffer-layers are compared with state-of-the-art NbN films of similar thicknesses on epitaxy supporting materials as 3C-SiC and MgO as seen Fig. (4.4).

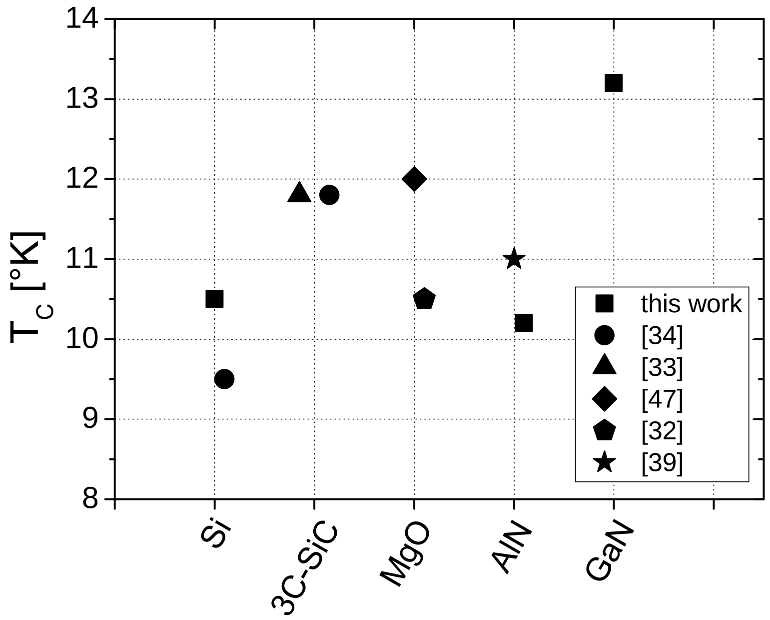


Figure 4.4: Reported NbN critical temperatures for ultra-thin films with 4.5-6nm thickness on different buffer-layer

First of all, it should be mentioned that the NbN films on silicon substrates deposited in the frame of this thesis reach similar Tc values as state-of-the-art depositions elsewhere. This testifies the quality of the developed in-house deposition process and constitute the importance of sensible process parameters as being discussed earlier. The NbN films grown onto GaN substrates indicate a highly prospective applicability in future THz electronics since it can be employed on thin membrane-like structures for wave-guide circuitry, does not degrade when stored in ambient atmosphere as the hydrophilic MgO does and furthermore exhibit a lower dielectric constant as seen from Tab. (2.2).

Also worth mentioning here is the predicted improvement of phonon transmission from NbN films to the substrates due to better acoustic matching and resulting faster HEB devices with enhanced IF bandwidth.

### 4.2.2 GaN epi-layer in contrast with bulk GaN

The growth of NbN on the applied GaN buffer-layer can be motivated from lattice crystal-structure considerations. All used AlGaN-composition exhibit a hexagonal crystal-structure or in particular a wurtzite-configuration as confirmed by the supplier ITME, Poland. However, NbN is ordered in a cubic fcc-phase and the lattice constant of bulk material of about a=4.4Å and a=4.46Å observed for high Tc thin-films [47]. Although, the most obvious orientation matching the lattice of AlGaN is the [111]-plane as seen from Fig. (4.5b,c) according $a_{111}=a_{100}\cdot/\sqrt{2} \approx 3.15$Å.

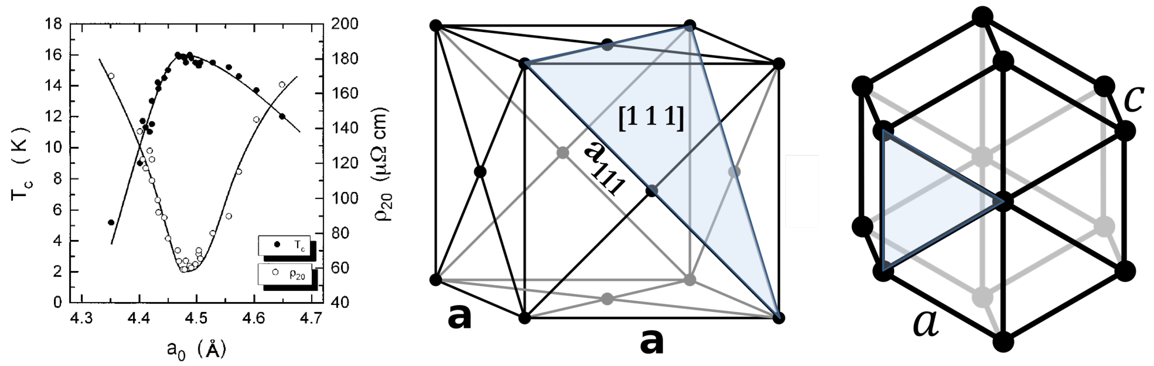


(a) NbN lattice versus Tc [47] (b) Cubic NbN lattice, source: http://chemwiki.ucdavis.edu (c) Hexagonal AlGaN, source: Daniel Mayer

Figure 4.5: Lattice constant of high Tc films and lattice of NbN and h-AlGaN

Furthermore, yet another experiments was conducted to justify the validity of the prospective GaN epilayer. Thus, NbN was grown both on bulk GaN also received from ITME, Poland and 1.2$\mu$m GaN/sapphire substrates in order to exclude that the favorable epitaxial growth arises from the underlying sapphire-substrate.

As clearly seen from Fig. (4.6) the out-standing critical temperatures of the NbN films have as well been repeated on bulk material and confirm the favorable properties of GaN substrates for future NbN superconductive electronics.

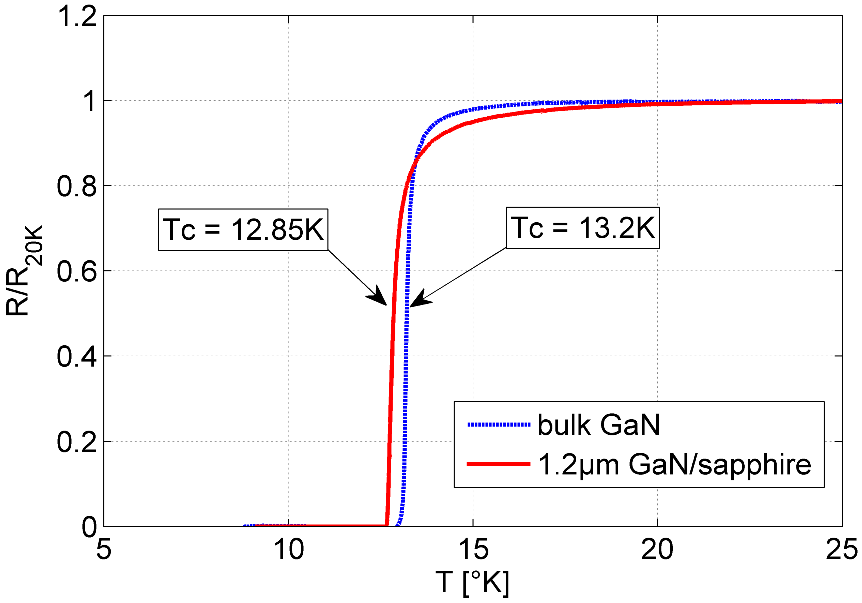


Figure 4.6: Critical temperature of a 5.5nm thin NbN film on bulk GaN and 1.2$\mu$m GaN epi-layer on sapphire, deposited simultaneously

## 4.3 Film-uniformity

The previously presented results are exceptionally promising for further investigation using micro-sized bolometer bridges in order to confirm the uniformity properties of films deposited on h-AlGaN buffer-layers. The bridges are distributed over the entire chip area and their resistance and critical temperatures of small probed areas will serve as an indicator for uniformity. The demand on high film uniformity arises from the fact that commonly used 2SB or balanced mixer require 2 identical mixer devices in order to effectively operate. The investigation of the film area by means of four-point-probe measurement gives sufficient and a time-effective indication of quality such as Tc, RRR and sheet resistance at normal-state, but since the probed area is fairly large, the current takes the path along best superconducting properties. Thus, it is important to confirm afore-mentioned properties on small probed areas throughout the entire film. The following illustrated processes were conducted in order to pattern the micro-bridges.

An image-reversal recipe has been utilized in order to define the pattern of feeding-lines and contact pads on top of the NbN film. This process involves a two-step exposure. Firstly, a short exposure time is chosen and a positive lithography achieved, Fig. (4.7b). After thermal treatment the pattern is reversed and would exhibit the edge-profile of a negative lithography process Fig. (4.7c). Subsequent flood exposure and developing removes the resist where the feeding-lines will be located later on Fig. (4.7c,d). The

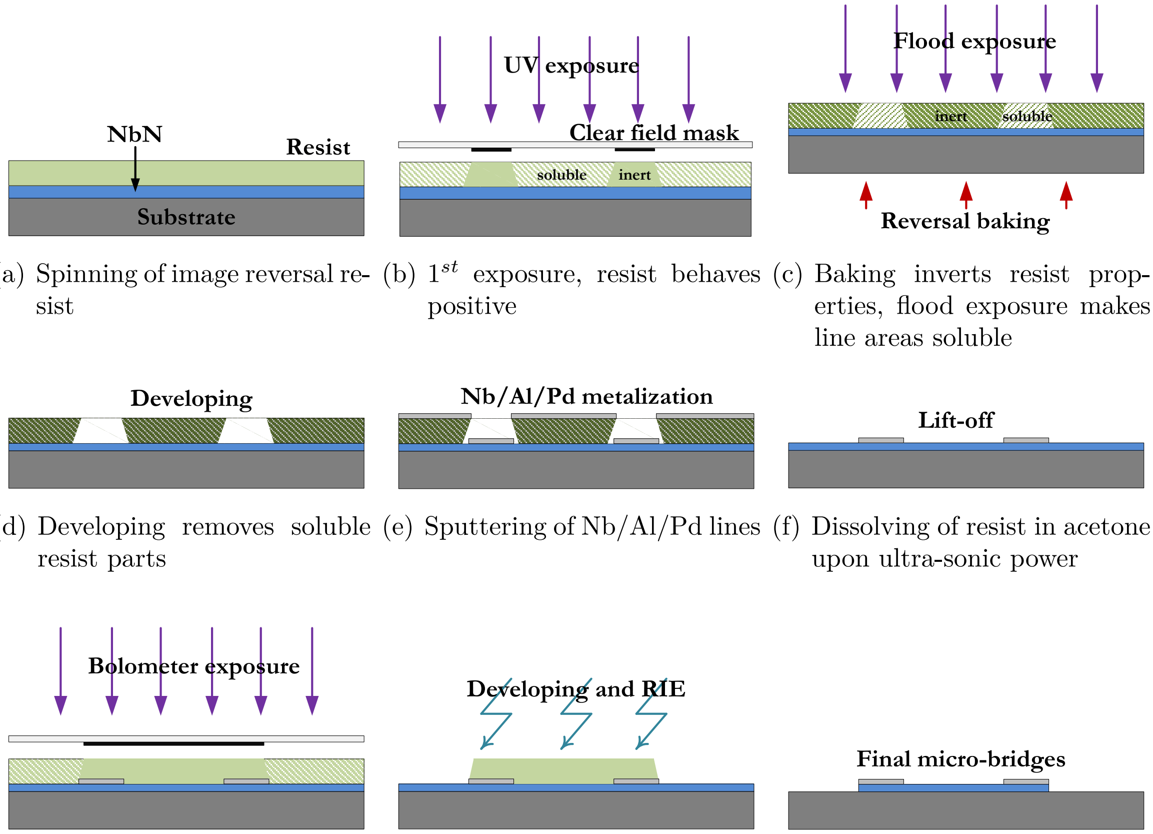


(a) Spinning of image reversal resist

(b) $1^{st}$ exposure, resist behaves positive

(c) Baking inverts resist properties, flood exposure makes line areas soluble

(d) Developing removes soluble resist parts

(e) Sputtering of Nb/Al/Pd lines

(f) Dissolving of resist in acetone upon ultra-sonic power

(g) $2^{nd}$ exposure of bolometer pattern

(h) Developing and etching of NbN by RIE

(i) Dicing and bonding of the processed structure

Figure 4.7: Process-flow of micro-bolometer fabrication by means of photo-lithography

deposition of a Nb/Al/Pd layered structure on top of the films takes place by means of DC magnetron sputtering Fig. (4.7e). The Nb-layer on top of NbN serves as an adhesion layer whereas the Al provide low resistivity of the lines and Pd on top is favorable for bonding the pads to the measurement setup. The metalization is found all over the film, although the areas covered with resist can be dissolved by acetone nonetheless due to the negative edge-profile Fig. (4.7f). The next step involves again the spinning of resist and proper alignment of micro-bridge like areas between the feeding-lines. Subsequently, exposure and development by means of a positive lithographic principle provide only resist on top of the NbN films where the bolometers will be, Fig. (4.7g). The last step depicts the process of Reactive Ion Etching RIE of the surrounding NbN, Fig. (4.7h,e)

As illustrated in Fig. (4.8) the transmission lines, contact pads as well as bolometers (purple) with dimensions ranging from 4x20$\mu$m to 5x5$\mu$m as well as 5x70$\mu$m to 20x70$\mu$m for critical current measurements have been fabricated.

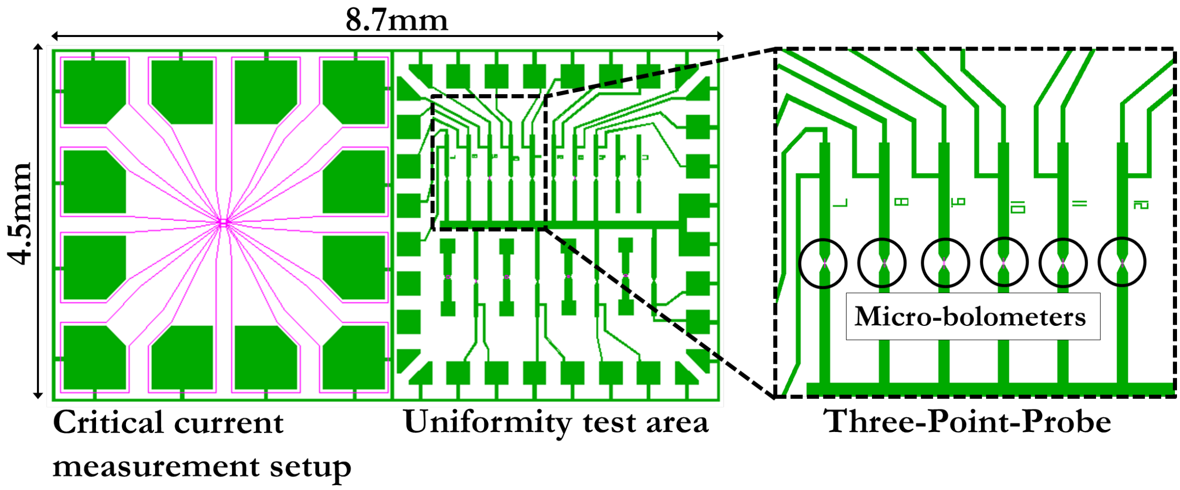


Figure 4.8: Micro-bridges of different sizes all over the film made by means of photo-lithography

Subsequently, the contact pads were bonded to a measurement fixture which provides connection to the current source and voltage read-out needed for the three-point-measurement. Moreover, it hosts a calibrated temperature sensor located in vicinity to the micro-bridge structure itself and allows accurate temperature sensing when slowly dipped into a LHe dewar. Resistance versus temperature curves were recorded separately for every bridge and evaluated as seen in Fig. (4.9).

The high uniformity could be confirmed for all different AlGaN buffer-layer materials ranging from 0 to 71% Al content. As seen from Tab. (4.1) a standard deviation of about 4-5% in sheet resistance and $\leq$0.56% in critical temperature was observed for all investigated bridge-sizes and lies inevitably within the uncertainties allowed for HEB device fabrication.

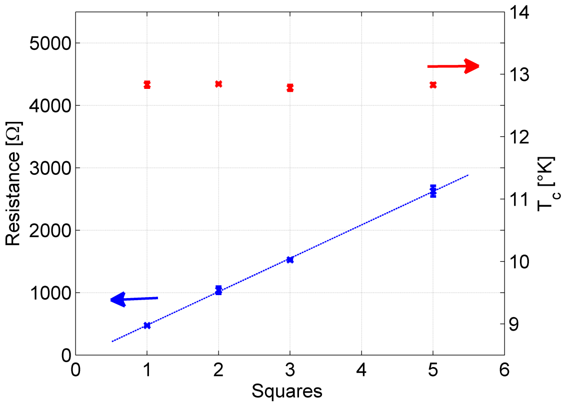


(a) GaN

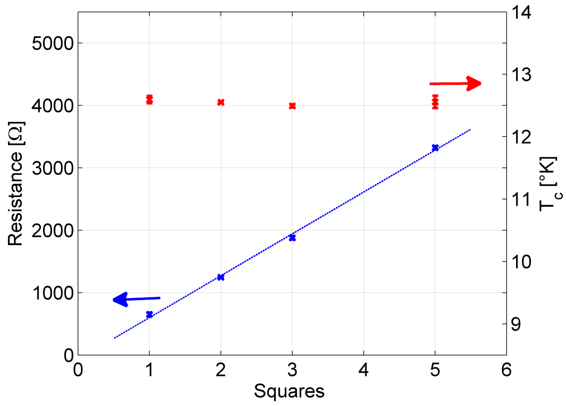


(b) $Al_{0.12}Ga_{0.88}N$

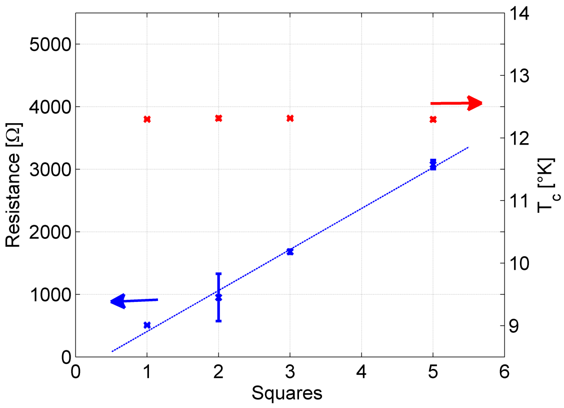


(c) $Al_{0.37}Ga_{0.63}N$

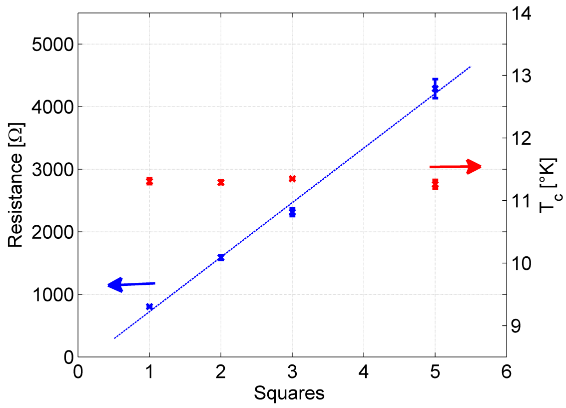


(d) $Al_{0.54}Ga_{0.46}N$

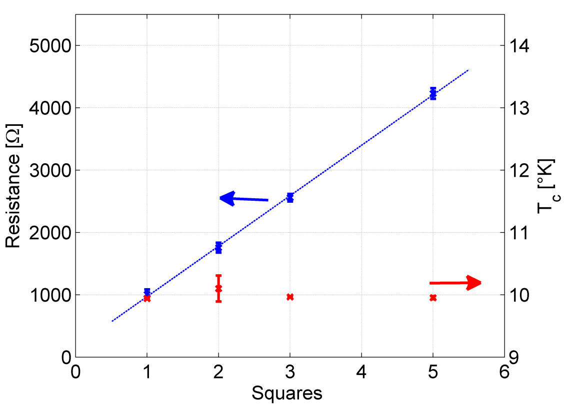


(e) $Al_{0.71}Ga_{0.29}N$

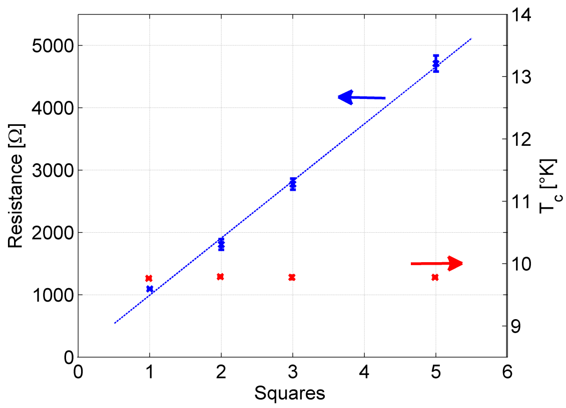


(f) Silicon

Figure 4.9: Resistance and Tc for various bridge sizes taken from a distributed film area (thickness ≈ 5.3nm), the deposition was conducted at elevated substrate temperatures

In addition, the films were stored about one month under ambient conditions in air before they were lithographically patterned, etched, bonded and re-measured. The observed degradation of the films in respect of critical temperature is about 0.15K and can be attributed to the protective properties of a thin $Nb_2O_5$ layer on top which was naturally formed and prevent further degradation.

| substrate | $R_\square$ at 20K | | Tc | | ΔTc | |
|---|---|---|---|---|---|---|
| | [Ω] | σ [%] | [K] | σ [%] | [K] | σ [%] |
| Silicon | 970±85 | 8.8 | 9.78±0.02 | 0.2 | 1.91±0.02 | 1.26 |
| $Al_{0.71}Ga_{0.29}N$ | 900±81 | 9 | 10.0 ±0.12 | 1.2 | 2.02±0.07 | 3.69 |
| $Al_{0.54}Ga_{0.46}N$ | 807±35 | 4.3 | 11.3 ±0.05 | 0.43 | 1.86±0.05 | 2.81 |
| $Al_{0.37}Ga_{0.63}N$ | 587±25.8 | 4.8 | 12.31±0.02 | 0.2 | 1.57±0.05 | 3.4 |
| $Al_{0.21}Ga_{0.79}N$ | 647±23 | 3.5 | 12.55±0.07 | 0.56 | 1.54±0.04 | 2.47 |
| GaN | 492±20 | 4 | 12.83±0.04 | 0.28 | 1.38±0.04 | 2.93 |

Table 4.1: Statistical summary of NbN micro-bridges on silicon and $Al_xGa_{1-x}N$-substrates deposited at elevated temperatures

Moreover, the superconducting properties of small micro-areas have also been studied for ambient deposited NbN films on both GaN and silicon substrates without intentional substrate heating. The fabrication of micro-bridges was the same as previously described.

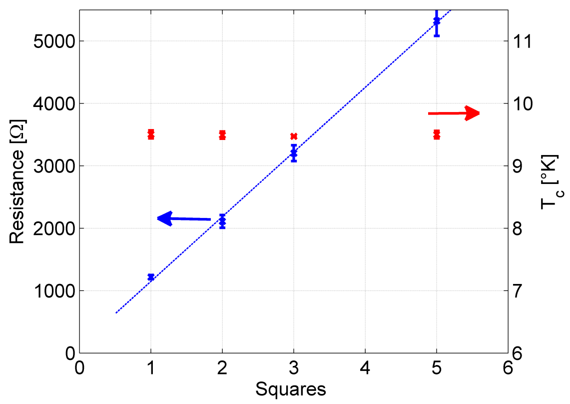


(a) GaN

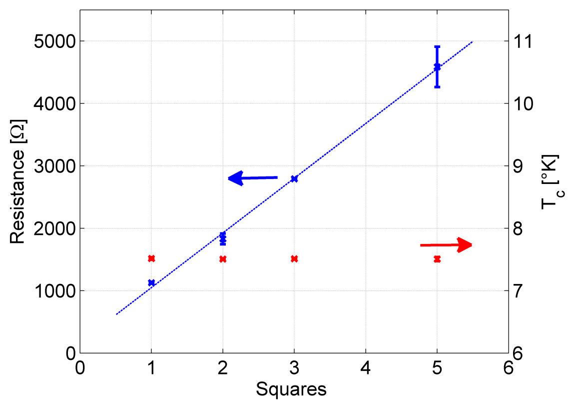


(b) SOI

Figure 4.10: Resistance and Tc for various bridge sizes deposited at ambient temperatures

The micro-bridges made on NbN/GaN feature a degradation of almost 1K in Tc as well as rise in sheet resistance after processing them. However, they still show an enhancement of 2K in critical temperature compared to the ones on silicon-substrates. Although, the uniformity could be validated as the standard deviation in Tc amounts to about 0.5% and in $R_\square$ to 7%.

| substrate | $R_\square$ at 20K | | Tc | | ΔTc | |
|---|---|---|---|---|---|---|
| | [Ω] | $\sigma$ [%] | [K] | $\sigma$ [%] | [K] | $\sigma$ [%] |
| Silicon | 981 ±99 | 7.5 | 7.51±0.02 | 0.26 | 1.53±0.02 | 1.32 |
| h-GaN | 1093±75 | 6.9 | 9.5±0.05 | 0.49 | 2.08±0.03 | 1.26 |

Table 4.2: Statistical summary of the micro-bridge characterization of cold deposited NbN films on GaN and silicon substrates

The growth of NbN at room temperature is desirable in respect to the employment of more complicated fabrication processes since photo-lithographic steps involving the use of resist can be performed prior deposition of NbN.

## 4.4 Critical Current Density Measurement

The critical current density as a function of temperature of NbN bridges both on hexagonal-GaN buffer layer and SOI was investigated and presented in Fig. (4.11). The dimensions of the tested bridges are 5.3nm x 10$\mu$m x 70$\mu$m in thickness, width and length, respectively and patterned by means of photo-lithography as illustrated in Fig. (4.8). The critical current was extracted from IV-curves taken in the range from 5K to the temperature they turn super-conductive and converted to a critical current density since the cross-section of the bridges is known.

The measured data was fitted to Eq. (4.1) and shows satisfying conformity with the simplified Ginzburg-Landau relationship [48].

$$j_c(T) = j_c(0) \cdot \left[1 - \left(\frac{T}{T_c}\right)^2\right]^{\frac{3}{2}} \tag{4.1}$$

By extracting the critical current density $j_{c0} = j_c|_{T=0}$ it turned out that an increase by almost a factor of 3 for the NbN film deposited onto a h-GaN buffer-layer compared to bare SOI has been achieved. This significant improvement of film's DC properties makes the GaN buffer-layer as well promising for other THz electronic applications such as single-photon detectors.

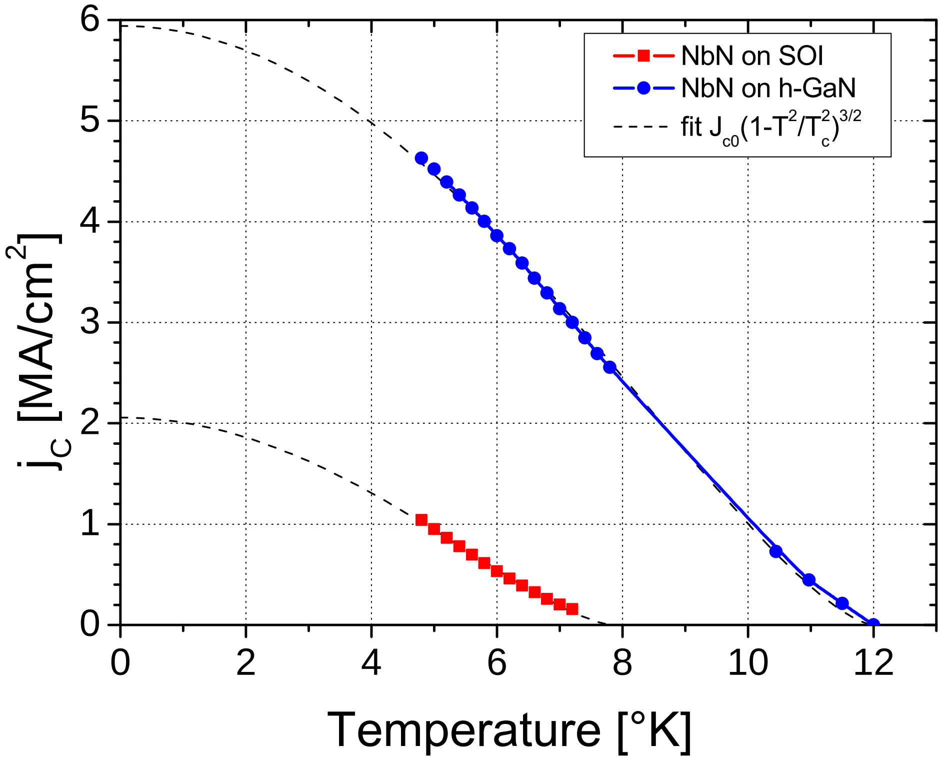


Figure 4.11: Critical current density versus temperature for ultra-thin NbN bridges grown on h-GaN and SOI substrates

## 4.5 Critical Magnetic Field Measurement

The dependence of critical temperature on an applied magnetic field reveals a deeper understanding of the super-conductive film properties and allows the estimation of physical properties as the diffusion coefficient D, coherence length $\xi$ and critical magnetic field $\mu H_{c2}$ according to the GLAG theory. The measurement itself was conducted in a manner that the film-resistance versus temperature was recorded under an applied magnetic field varied stepwise from 0 to 14Tesla. Subsequently, the critical temperature was extracted from the R(T) curves and plotted versus the magnetic field as illustrated in Fig. (4.12).

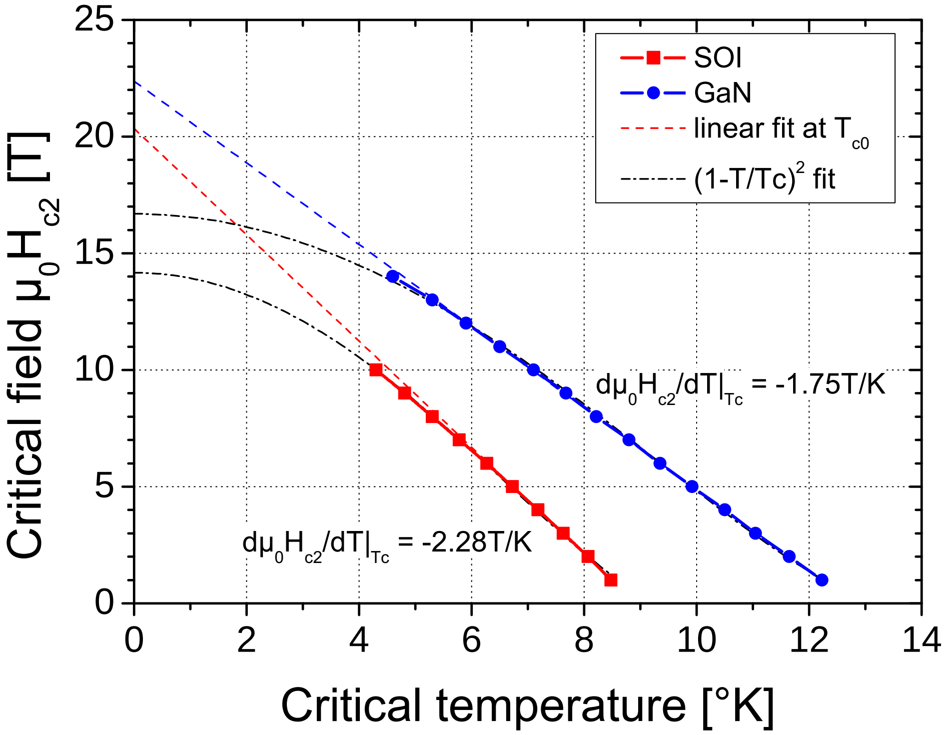


Figure 4.12: Critical temperature dependence on magnetic field perpendicular to the NbN bridges grown on h-GaN and SOI substrates

The measurement points have been fitted to the expected quadratical behavior Eq. (4.2) according to [48] and yield to a second critical magnetic field $\mu_0 \mathrm{H}_{c2}(0)$ of about 17T and 14T for NbN on h-GaN and SOI, respectively.

$$B_c(T) = B_c(0) \cdot \left[1 - \left(\frac{T}{T_c}\right)^2\right] \tag{4.2}$$

The diffusion coefficients represents the ability of electrons to exchange their energy by means of diffusion under a temperature gradient and can be estimated by Eq. (4.3).

$$D \approx 10^4 \left[-\frac{d\mu_0 H_{c2}}{dT}\bigg|_{Tc}\right]^{-1} \tag{4.3}$$

Applying the derivative of the critical magnetic field over the critical temperature in the vicinity of Tc in Eq. (4.3) D=0.44cm$^2$/s is obtained for our silicon samples which is in accordance with reported values of 0.4cm$^2$/s [49]. In contrast the NbN film deposited onto GaN substrate reaches a diffusion coefficient of 0.57cm$^2$/s.
The improvement of electron's diffusivity on GaN substrates can be employed in utilizing an additional diffusion channel in phonon-cooled HEB mixers as recently demonstrated [50], [51].

# 5 Conclusion and future outlook

Within the frame of this thesis, prospective buffer-layers such as $Al_xGa_{1-x}N$ have been investigated for the deposition of ultra-thin NbN films by means of reactive DC magnetron sputtering. As a result, state-of-the-art NbN films with thickness of about 5.5nm have been grown on hexagonal GaN substrate and exhibit Tc as high as 13.2K and RRR close to unity, which is evidence of an epitaxial growth.
The uniformity was confirmed by R(T)-measurements of micro-bridge areas across the entire film, processed by means of micro-fabrication. The standard-deviation of sheet resistance was about 4% and thus even lower than for well-established bare-silicon substrates of about 8%. Furthermore, it has been observed that the increase of Al-content above 20% in $Al_xGa_{1-x}N$ epi-layer gradually deteriorates the super-conducting properties of NbN down to values similar to the one achieved on silicon substrates. The critical current density was measured and amounts to about 6MA/cm$^2$ on GaN and 2MAcm$^2$ on silicon-substrates which highlights the improved superconducting properties. Process parameter optimization for the deposition of NbN ultra-thin films has been carried out on SOI substrates, reaching Tc of 10.5K and turned out to be applied on arbitrary substrates. The most influence on film's quality was exerted by the substrate temperature, an accurate $N_2$/Ar ratio determining NbN's stoichiometry, the process pressure, applied RF bias while sputtering as well as purging still heated films with Ar post-deposition.
Moreover, the deposition of NbN without intensionally substrate heating was demonstrated and show after processing of micro-bridges still Tc of 9.5K compared to 7.5K on silicon for about 5.5nm thin films.

Furthermore, a theoretical emphasis was on the employment of buffer-layers for HEB heterodyne mixers in order to improve their limited IF bandwidth, which is of major concern for efficient astronomical observations in the THz regime. From studies on acoustic matching between superconducting thin-films and substrate [3] one can deduce a prospective enhancement of HEB's IF bandwidth using GaN substrates as stated below.

- High Tc and epitaxial growth
  The exchange of energy from hot electrons to phonons is $\tau_{eph} \propto \mathrm{T}^{-1.6}$ which promotes the cooling of hot electrons upon radiation → increase of IF bandwidth
- Acoustic matching of NbN film and substrate
  The high density and relatively low acoustic velocity of GaN compared to usually employed substrates as Si, 3C-SiC, MgO, sapphire increases the phonon transmission coefficient [3] and prevents the trapping of phonons at the interface as well as reduces the escape time of phonons to the substrate → increase of IF bandwidth
- Additional diffusion channel to phonon-cooled HEB proposed in [50]
  Recent demonstrations of utilizing an additional diffusion channel for electrons in phonon-cooled HEB on silicon increased the IF bandwidth up to 8GHz. Enhanced diffusivity of electrons in NbN on GaN-substrates 0.57cm$^2$/s compared to bare silicon-substrates 0.4cm$^2$/s have been shown by means of critical magnetic field measurement and would promote the diffusion cooling concept even more

The future work will mainly consist of employing this promising material for the epitaxial growth of NbN and confirm fore-casted enhancement as increased IF bandwidth in HEB mixers. Terahertz electronics as SIS tunnel junctions or Single Photon Detectors could also benefit from the high-quality growth of NbN in order to extend the operating frequency and sensitivity, respectively. Due to its obvious lattice match to GaN one can also think of employing NbN buffer-layer and support the growth of high-quality GaN which in fact is widely used in blue laserdiode or LED as well as power transistors due to its wide band-gap.

# Bibliography


[1] D. Meledin, A. Pavolotsky, V. Desmaris, I. Lapkin, C. Risacher, V. Perez, D. Henke, O. Nystrom, E. Sundin, D. Dochev, M. Pantaleev, M. Fredrixon, M. Strandberg, B. Voronov, G. Goltsman, V. Belitsky: *A 1.3-THz Balanced Waveguide HEB Mixer for the APEX Telescope*. IEEE Transactions on Microwave Theory and Techniques, Vol. 57, No. 1, 2009.

[2] R. Silberg: *HIFI instrument*. http://herschel.jpl.nasa.gov/hifiInstrument.

[3] S. Kaplan: *Acoustic Matching of Superconducting Films to Substrates*. Journal of Low Temperature Physics, Vol. 37, No. 3/4, 1979.

[4] C. Kulesa: *Terahertz Spectroscopy for Astronomy: From Comets to Cosmology*. IEEE Transactions on Terahertz Science and Technology, Vol. 1, No. 1, 2011.

[5] C. Armstrong: *The Truth About Terahertz*. IEEE Spectrum, 2012.

[6] F. Sizov, A. Rogalski: *Thz Detectors*. Progress in Quantum Electronics 34, pp.278-347, 2010.

[7] A. Semenov, H. Richter, H. Hübers, A. Kuzmin, K. Ilin, M.. Siegel, D. Petrenko, I. Tretyakov, S. Ryabchun, M. Finkel, N. Kaurova, G. Gol'tsman. : *Optimization of the intermediate frequency bandwidth in the THz HEB mixers*. 24th International Syposium on Space Terahertz Technology, 2013.

[8] K. Ilin, R. Schneider, D. Gerthsen, A. Engel, H. Bartolf, A. Schilling, A. Semenov, H-W. Huebers, B. Freitag, M. Siegel: *Ultathin NbN films on Si: crystalline and superconducting properties*. Journal of Physics: Conference Series 97, 2008.

[9] A. Woodcraft, M. Hollister, D. Bintley, M. Ellis, X. Gao, W. Holland: *Characterization of a prototype SCUBA-2 1280-pixel submillimetre superconducting bolometer array*. Proceedings SPIE, Vol. 6275,2006.

[10] S. Lin, O. Ayala-Valenzuela, R. McDonald, L. Bulaevskii, T. Holesinger, F. Ronning, N. Weisse-Bernstein, T. Williamson, A. Mueller, M. Hoffbauer, M. Rabin, M. Graf: *Characterization of thin-film NbN superconductor for single-photon detection by transport measurements*. Physical Review B, 87, 184507, 2013.

[11] E. Gershenzon, G. Gol'tsman, I. Gogidze, Y. Gusev, A. Elant'ev, B. Karasik, A. Semenov : *Millimeter and submillimeter range mixer based on electronic heating of superconducting films in the resistive state*. Superconductivity: Physics, Chemistry, Technology, Vol. 3, No. 10, pp.1582-1597, 1990.

[12] D. Prober: *Superconducting terahertz mixer using a transition-edge microbolometer*. Applied Physics Letter, Vol. 62, 1993.

[13] K. II'in, I. Milostnaya, A. Verevkin, G. Gol'tsman, E. Gershenzon, R. Sobolewski: *Ultimate quantum efficiency of a superconducting hot-electron photodetector*. Applied Physics Letter, Vol. 73, No. 26, 1998.

[14] K. II'in, I. Milostnaya, A. Verevkin, G. Gol'tsman, E. Gershenzon, R. Sobolewski: *Picosecond hot-electron energy relaxation in NbN superconducting photodetectors*. Applied Physics Letter, Vol. 76, No. 19, 2000.

[15] N. Perrin, C. Vanneste: *Response of superconducting films to a periodic optical irradiation*. Physical Review B, Vol. 28, Nr. 9, 1983.

[16] A. Semenov, R. Nebosis, Y. Gousev, M. Heusinger, K. Renk: *Analysis of the nonequilibrium photoresponse of superconducting films to pulsed radiation by use of a two-temperature model*. Physical Review B, Vol. 52, No. 1, 1995.

[17] R. Nebosis, A. Semenov, Y. Gousev, K. Renk:*Rigorous Analysis of a Superconducting Hot-Electron Bolometer Mixer:Theory and Comparison with Experiment*.$7^{th}$International Symposium on Space Terahertz Technology, 1996.

[18] A. Sergeev, B. Karasikb, M. Gershenson, V. Mitin: *Electron-phonon scattering in disordered metallic films*. Physica B, pp. 316-317,328-330, 2002.

[19] A. Sergeev, M. Reizer: *Photoresponse Mechanisms of Thin Superconducting Films and Superconducting Detectors*. International Journal of Modern Physics B, Vol. 10, No. 6, pp. 635-667, 1996.

[20] N. Ptitsina, G. Chulkova, K. Il'in, A. Sergeev, F. Pochinkov, E. Gershenzon, M. Gershenzon: *Electron-phonon interaction in disordered*

*metal films: The resistivity and electron dephasing rate.* Physical Review B, Vol. 56, No. 16, 1997.

[21] J. Kooi, J. Baselmans, M. hajenius, J. Gao, T. klapwijk, P. Dieleman, A. Baryshev, G. de Lange: *IF impedance and mixer gain of NbN hot electron bolometer.* Journal of Applied Physics Vol.101, 044511, 2007.

[22] Yu. Gousev, G. Gol'tsman, A. Semenov, E. Gershenzon, R. Nebosis, M. Heusinger, K. Renk.: *Broadband ultrafast superconducting NbN detector for electromagnetic radiation.* Journal of Applied Physics Vol. 75, No. 7, 1994.

[23] K. Il'in, M. Lindgren, M. Currie, A. Semenov, G. Gol'tsman, R. Sobolewski, S. Cherednichenko, E. Gershenzon: *Picosencond hot-electron relaxation in NbN superconducting photodetectors.* Applied Physics Letters, Vol. 76, No. 19, 2000.

[24] S. Chockalingam,M. Chand,J. Jesudasan,V. Tripathi,P. Raychaudhuri: *Superconducting properties and Hall effect of epitaxial NbN thin films.* Physical Review B, Vol. 77, 214503, 2008.

[25] A.Ghosh, H.Weismann, M.Gurvitch, H.Lutz, O. Kammerer, C. Snead, A. Goland, M. Strongin: *The Effects of Irradiation at Cryogenic Temperatures and Electron Irradiation on Tc and the Transport Properties of A-15 Super-conductors.* Journal of Nuclear Materials, Vol. 72, pp. 70-75, 1978.

[26] R. Da-Hua, C. Xin-Lu: *First-principles calculations on the elastic and thermodynamic properties of NbN.* Chin. Phys. B Vol. 21, No. 12, 2012.

[27] T. Amrioua, B. Bouhafsa, H. Aouraga, B. Khelifab, S. Bressonb, C. Mathieu: *FP-LAPW investigations of electronic structure and bonding mechanism of NbC and NbN compounds.* Physica B, 325, pp. 46-56, 2003.

[28] J. Kim, J. Achenbach, P. Mirkarimi, M. Shinn, S. Barnett: *Elastic constants of single-crystal transition-metal nitride films measured by line-focus acoustic microscopy.* Journal of Applied Physics Vol. 72, 1805, 1992.

[29] Z.-H. Wang, X.-Y. Kuang, X.-F. Huang, P. Lu, A.-J Mao: *Pressure-induced structural transition and thermodynamic properties of NbN and effect of metallic bonding on its hardness.* EPL, 92, 2010.

[30] L. Kang, B. Jin, X. liu, X. Jia, J. Chen: *Suppression of superconductivity in epitaxial NbN ultrathin films.* Journal of Applied Physics, Vol. 109, 2011.

[31] R. Espiau de Lamaestre, Ph. Odier, E. Bellet-Amalric, P. Cavalier, S. Pouget, J. Villegier: *High quality ultrathin NbN layers on sapphire for superconducting single photon detectors*. Journal of Physics: Conference Series 97, 012046, 2008.

[32] A. Kawakami, S. Tanaka, M. Yasui, I. Hosako, Y. Irimajiri : *Design and Fabrication of NbN Terahertz Hot Electron Bolometer Mixers*. 24th International Syposium on Space Terahertz Technology, 2013.

[33] D. Dochev, V. Desmaris, A. Pavolotsky, D. Meledin, Z. Lai, A. Henry, E. Janzen, E. Pippel, J. Woltersdorf, V. Belitsky: *Growth and Characterization of Epitaxial Ultra-Thin NbN Films on 3C-SiC/Si substrates for Terahertz Applications*. Superconductor Science and Technology, 24, 2010.

[34] J. Gao, M. Hajenius, F. Tichelaar, T. Klapwijk, B. Voronov, E. Grishin, G. Gol'tsman, C. Zorman, M. Mehregany: *Monocrystalline NbN nanofilms on a 3C-SiC/Si substrate*. Applied Physics Letters, Vol. 91, 062504, 2007.

[35] C. Deger, E. Born, H. Angerer, O. Ambacher, M. Stutzmann: *Sound velocity of $Al_xGa_{1-x}N$ thin films obtained by surface acoustic-wave measurements*. Applied Physics Letters, 72, 2400, 1998.

[36] J. Winey, Y. Gupta, D. Hare: *r-axis sound speed and elastic properties of sapphire single crystals*. Journal of Applied Physics, Vol. 90, 3109, 2001.

[37] A. Gleason, H. Marquardt, B. Chen, S. Speziale, J. Wu, R. Jeanloz: *Anomalous sound velocities in polycrystalline MgO under nonhydrostatic compression*.Geophysical Research Letters, Vol. 38, L03304, 2011.

[38] C. Zha, R. Hemley, H. Mao, T. Duffy, C. Meade: *Acoustic velocities and refractive index of $SiO_2$ glass to 57.5GPa by Brillouin scattering*. Physical Review B, Condensed Matter, 3rd series, Vol. 50, Nr. 18. 1994.

[39] T. Shino, S. Shiba, N. Sakai, T. Yamakura, L. Jiang, Y. Uzawa, H. Maezawa, S. Yamamoto: *Improvement of Critical Temperature of Superconducting NbTiN and NbN Thin Films Using the AlN Buffer Layer*. Submitted to: Supercond. Sci. Technol., PACS numbers: 74.78.-w.

[40] X. Li, R. Yang: *Effect of lattice mismatch on phonon transmission and interface thermal conductance across dissimilar material interfaces*. Physical Review B 86, 2012.

[41] W. Lengauer, M. Bohn, B. Wollein, K. Lisak: *Phase reactions in the Nb-N system below 1400°*. Acta mater. 48, 2633-2638, 2000.

[42] G. Eremeev: *Review of RF Properties of NbN and $MgB_2$ thin coating on Nb samples and cavities*. Proceedings of SRF2009, Berlin, Germany, 2009.

[43] D. capone, K. Gray, R. Kampwirth: *New scaling relation for sputtered NbN films*. Journal of Applied Physics, Vol. 65, pp. 258-261, 1989.

[44] I. Hotovy, R. Srnanek, D. Buc: *Effects of thermal annealing on the properties of niobium nitride thin films*. Journal of Materials Science Letters13, 1226-1228, 1994.

[45] M. Hatano, T. Nishino, U. Kawabe: *Effects of thermal annealing of superconduction Nb and NbN films*. Journal of Vacuum Science and Technology, A 6, 2381, 1988.

[46] K. Tanabe, H. Asano, Y. Katoh, O. Michikami: *Ellipsometry and optical reflectivity studies of reactively sputtered NbN thin films*. Journal of Applied Physics Vol. 63, No. 5, 1988.

[47] Z. Wang, A. Kawakami, Y. Uzawa, B. Komiyama: *Superconducting properties and crystal structures of singlecrystal niobium nitride thin films deposited at ambient substrate temperature*. Journal of Applied Physics, Vol. 79, 7837, 1996.

[48] M. Cyrot: *Ginzburg-Landau theory for supercondcutors*. Rep. Prog. Phys. 36, 103, 1973.

[49] D. Floet, J. Gao, T. Klapwijk, P. Korte: *Thermal time constant of Nb diffusion-cooled superconducting hot-electron bolometer mixers*. IEEE Trans. Appl. Supercond., Vol. 11, pp. 187-190, 2001.

[50] S. Ryabchun, I. Tretyakov, M. Finkel, S. Maslennikov, N. Kaurova, V. Seleznev, B. Voronov, G. Gol'tsman: *Fabrication and characterization of NbN HEB mixers with in situ gold contacts*. 19th International Symposium on Space Terahertz Technology, Groningen, 2008.

[51] M. Finkel, Y. Vachtomin, S. Antipov, V. Drakinski, N. Kaurova, B. Voronov, G. Goltsman: *Gain Bandwidth and Nioise Temperature of NbTiN HEB Mixers*. 14th International Symposium on Space Terahertz Technology, 2003.